Cellular and Molecular Life Sciences (2026) 83:74
https://doi.org/10.1007/s00018-025-06019-7

ORIGINAL ARTICLE

The pathway-independent positive allosteric modulator C1 allows for the identification of active Y_4 receptor relevant positions

Corinna Schüß[1] · Oanh Vu[2] · Tim Pelczyk[1] · Mario Schubert[1,3] · Yu Du[4] · Jan Stichel[1] · C. David Weaver[4,5] · Jens Meiler[2,6] · Annette G. Beck-Sickinger[1]

Received: 21 July 2025 / Revised: 5 November 2025 / Accepted: 17 November 2025
© The Author(s) 2025

Abstract

The neuropeptide Y_4 receptor (Y_4R) and its endogenous ligand pancreatic polypeptide (PP) are primarily involved in the regulation of satiety and energy balance and present relevant pharmacological targets. We characterized the novel Y_4R positive allosteric modulator C1 that enhances Y_4R G-protein signaling, ligand binding, and arrestin-3 recruitment to Y_4R. Comparison with a close analog revealed the structural importance of an ethyl acetate moiety for Y_4R affinity and PAM activity at the G-protein pathway. C1 shows a high selectivity for the Y_4R, while signaling of the related subtypes Y_1R, Y_2R, and Y_5R is not affected. Y_4R G-protein signaling is even potentiated by the low-affinity agonists neuropeptide Y and peptide YY. Binding affinity of the endogenous ligands to Y_4R is enhanced by C1, indicating a stabilization of the ligand-bound Y_4R conformation. Using Y_4R/Y_1R chimera, important Y_4R domains for C1 activity were identified. Single point mutagenesis and computational docking pinpointed hot-spot residues at Y_4R important for stabilizing the active ligand-bound conformation.

Keywords Neuropeptide Y_4 receptor · Allostery · Pancreatic polypeptide · Mutagenesis · Receptor pharmacology · GPCR modulation

Abbreviations

BRET	bioluminescence resonance energy transfer
COS-7	African green monkey kidney cells
CRC	concentration-response curve
DMEM	Dulbecco's modified Eagle's medium
DPBS	Dulbecco's phosphate-buffered saline
ECL	extracellular loop
eYFP	enhanced yellow fluorescent protein
FBS	fetal bovine serum
HBSS	Hank's balanced saline solution
HEK293	human embryonic kidney cells
ICL	intracellular loop
K_B	equilibrium binding constant
M2R	M2 muscarinic receptor
mGlu2R	metabotropic glutamate 2 receptor
NPY	neuropeptide Y
PP	pancreatic polypeptide
PYY	peptide YY
RP-HPLC	reversed-phase high-performance liquid chromatography
SEM	standard error of the mean
TM	transmembrane
$Y_{1/2/4/5}R$	neuropeptide Y receptor subtype 1/2/4/5

✉ Corinna Schüß
corinna.schuess@uni-leipzig.de

1 Institute of Biochemistry, Leipzig University, 04103 Leipzig, Germany

2 Department of Chemistry, Vanderbilt University, Nashville, TN 37235, USA

3 Institute of Pharmacology and Toxicology, Technische Universität Dresden, 01307 Dresden, Germany

4 Department of Pharmacology, Vanderbilt University, Nashville, TN 37232, USA

5 Institute of Chemical Biology, Vanderbilt University, Nashville, TN 37232, USA

6 Institute for Drug Discovery, Leipzig University, 04103 Leipzig, Germany

Published online: 13 January 2026

Introduction

G protein-coupled receptors (GPCRs) represent a large and highly heterogeneous superfamily of cell surface receptors. They orchestrate numerous cellular functions in response to a versatile set of ligands [1]. GPCRs have emerged as major therapeutic targets and have become a central element in drug discovery in recent decades [2, 3]. Peptide-activated GPCRs are of particular interest as 32% of rhodopsin-like GPCRs naturally bind to peptides. Most drugs targeting peptide GPCRs that are either approved or under development are used for the treatment of metabolic diseases and cancer [4, 5]. Conventional GPCR-based drug discovery strategies have revolved around developing ligands based on the structure of native agonists or antagonists targeting the orthosteric site of a receptor [6], which are well characterized for many GPCRs, including the neuropeptide Y_4 receptor (Y_4R) [7]. In this study, we aim to understand receptor activation by characterizing a novel small-molecule ligand for Y_4R. This allows us to broaden the pharmacological toolbox, complementing large peptide ligands, and opening new avenues in peptide GPCR drug discovery [6, 8–10]. Allosteric modulators of GPCRs have gained increasing attention, especially since three allosteric modulators, maraviroc, cinacalcet and, avacopan, have already made it to the clinic [11–14] and several more are under investigation in clinical trials [15]. Furthermore, advancements in high-throughput screening (HTS) technologies, structural elucidation, and computational methodologies will advance the rational and structure-based development of novel GPCR allosteric drugs within the near future [16, 17].

This study investigates the allosteric mechanism and binding pocket of a novel positive allosteric modulator (PAM) of the Y_4R, termed C1 (VU0610218). The Y_4R, a peptide GPCR mainly expressed in the gastrointestinal tract, regulates satiety and energy expenditure upon stimulation by its endogenous ligand pancreatic polypeptide (PP) [18–21]. Previous studies have demonstrated that activation of Y_4R with selective agonists induces weight loss in mice [22–24] and reduces food intake in humans [25, 26]. Consequently, positive modulation of PP-mediated Y_4R response emerges as a promising approach to augment the physiological signaling, and advance the Y_4R as clinically relevant GPCR. Previously, niclosamide and tBPC have been identified as Y_4R positive allosteric modulators, however, these compounds exhibit limited selectivity or show agonistic activity at Y_4R in the absence of the endogenous peptide ligands [27, 28]. In this study, C1 was identified as structurally novel Y_4R pure PAM in a Ca^{2+} flux-based high-throughput screening (HTS). The Y_4R is part of a multiligand/multireceptor system comprising the closely related receptors Y_1R, Y_2R, and Y_5R and the peptide ligands PP, peptide YY (PYY) and neuropeptide Y (NPY) [29]. Therefore, the effect of the small molecule C1 and its analog C2 was also investigated for Y receptor selectivity and functional ligand selectivity. Using different functional assay set-ups, we aim to understand the molecular mechanism of this small molecule at Y_4R with respect to G-protein signaling and binding. As Y_4R promiscuously couples to different intracellular signaling proteins, the effect of C1 on arrestin recruitment to Y_4R is considered in addition to the G-protein pathway. By mutagenesis approaches using Y_4R/Y_1R chimeras and single mutants, as well as computational docking using the recently described Y_4R-PP-G_{i1} cryo-electron microscopy (cryo-EM) structure [7], we present the allosteric binding pocket of C1 at the active state of Y_4R.

Materials and methods

Material

Molecular biology and functional assays Dulbecco's Modified Eagle's Medium (DMEM), Hank's Balanced Salt Solution (HBSS), Dulbecco's Phosphate-Buffered Saline (DPBS), trypsin-EDTA, and Ham's F12 were obtained from Lonza (Basel, Switzerland). DMEM/F-12 medium without phenol red was purchased from Gibco™, Thermo Fisher (Waltham, MA, USA). G418 sulfate and hygromycin B were from Invivogen (Toulouse, France). Fetal bovine serum (FBS) was purchased from Biochrom GmbH (Berlin, Germany). OptiMEM was received from Life Technologies (Basel, Switzerland). Dimethylsulfoxide (DMSO), Pluronic F-127, HEPES, Hoechst33342, probenecid, forskolin, TRIS, polyethylenimine, Pefabloc, calium chloride ($CaCl_2$) and magnesium chloride ($MgCl_2$) were purchased from Sigma-Aldrich (St. Louis, MO, USA). Bovine serum albumin (BSA) was obtained from Carl Roth (Karlsruhe, Germany). MetafectenePro transfection reagent was acquired from Biontex Laboratories GmbH (München, Germany). Lipofectamine™ 2000 transfection reagent and competent *Escherichia coli* (*E.coli*) DH5α were purchased from Invitrogen (Carlsbad, CA, USA). Coelenterazine h was received from NanoLight Technology (Pinetop, AZ, USA). Fluo-2 AM was from Abcam (Cambridge, UK). GloSensor cAMP reagent was obtained from Promega (Fitchburg, WI, USA). Human ^{125}I–PP and ^{125}I–PYY were purchased from PerkinElmer (Waltham, MA, USA). *DpnI*, deoxyribonucleotide (dNTP) mix, Phusion High-Fidelity Polymerase, and 5× HF buffer were obtained from Thermo Fisher Scientific (Waltham, MA, USA). Sense and antisense primers were purchased from Biomers (Ulm, Germany). Wizard Plus

Mini and Midi DNA purification kits were purchased from Promega (Fitchburg, WI, USA).

Compounds C1 (VU0610218, product ID: F3315-0069) and C2 (product ID: F3315-0071) were ordered from Life Chemicals (Kyiv, Ukraine). All compounds are > 95% pure by HPLC (Fig. S6).

Plasmids

For signaling studies, the coding sequence of human Y_4R, C-terminally fused to eYFP, was cloned into the mammalian expression vector pEYFP_N1 (Clontech, Heidelberg, Germany), and pVitro2-hygro-mcs vector (Invivogen), as described in earlier studies [30, 31]. The chimeric G protein $\Delta 6G\alpha_{qi4-myr}$ was kindly provided by Evi Kostenis (Rheinische Friedrich-Wilhelms-Universität, Bonn, Germany) [32]. Arrestin BRET was performed with bovine arrestin-3, N-terminally tagged with Venus fluorophore, and Y_4R, C-terminally fused to *Renilla* luciferase 8 and cloned into the pcDNA3 vector [33, 34]. The pGloSensor-22 F cAMP plasmid (Cat. # E2301) was obtained from Promega (Fitchburg, WI, USA). The G protein sensors (G_{o1}-CASE RRID: Addgene_168123, G_{i3}-CASE RRID: Addgene_168122) were kindly provided by Hannes Schihada and Gunnar Schulte (Karolinska Institute, Stockholm, Sweden).

Mutagenesis

Single amino acid substitutions or segments of 2–4 adjacent residues were introduced into wildtype Y_4R-eYFP_N1 plasmid by site-directed mutagenesis PCR using Phusion High-Fidelity Polymerase and 5× HF buffer according to the manufacturer's protocol. Sense and antisense primers were used at a final concentration of 0.5 µM, and dNTP mix was added at a final concentration of 200 µM. *DpnI* was used to digest parental methylated DNA for 3 h at 37 °C. PureYield Plasmid MiniPrep and MidiPrep DNA Purification Kits were used to isolate plasmid DNA after transformation of the cDNA into competent *E.coli* DH5α, as recently described [35]. The sequence of all Y_4R mutant constructs was confirmed by Sanger dideoxy sequencing. Membrane expression and signaling of Y_4R variants was investigated by live cell microscopy and are summarized in Fig. S3 and [35].

Cell culture

All cell lines were cultivated in 75 cm^2 cell culture flasks in a humidified atmosphere at 37 °C and 5% CO_2, and passaged twice a week. The stable cell lines COS-7_$hY_{1/2/4/5}R$-eYFP_$\Delta 6G\alpha_{qi4-myr}$, co-expressing either Y_1R, Y_2R, Y_4R, or Y_5R, C-terminally fused to eYFP fluorophore, and the chimeric G protein $\Delta 6G\alpha_{qi4-myr}$ were maintained in DMEM supplemented with 10% heat-inactivated FBS, 133 µg/mL hygromycin B, and 1.5 mg/mL G418 sulfate. Wildtype COS-7 cells were obtained from the American Type Culture Collection (ATCC, Manassas, VA, USA; CRL-1651, RRID: CVCL_0224ATCC) and cultured in DMEM supplemented with 10% heat-inactivated FBS. HEK293 cells, obtained from the Deutsche Sammlung von Mikroorganismen und Zellkulturen (DSMZ, Braunschweig, Germany; ACC-305, RRID: CVCL_0045), were cultured in DMEM/Ham's F12 medium (1:1 *v/v*) supplemented with 15% heat-inactivated FBS. Stably transfected HEK293-hY_4R-eYFP cells were maintained in DMEM/Ham's F12 medium (1:1 *v/v)*, 15% heat-inactivated FBS, and 100 µg/mL hygromycin. All cell lines were routinely tested negative for mycoplasma contamination.

Ca^{2+} flux assay

Ca^{2+} flux assays were performed in COS-7 cells stably co-expressing hY_4R-eYFP and the G protein chimera $\Delta 6G\alpha_{qi4-myr}$, as previously described [35]. Compound selectivity studies were performed in stably transfected COS-7_$hY_{1/2/5}R$-eYFP_$\Delta 6G\alpha_{qi4-myr}$ cells. For mutagenesis studies, COS-7 cells were transiently co-transfected with Y_4R-eYFP WT or mutant plasmid, and the chimeric G protein $\Delta 6G\alpha_{qi4-myr}$ (ratio 3:1) overnight using Metafectene Pro transfection reagent, according to the manufacturer's protocol. Transiently or stably transfected COS-7 cells were seeded in black clear bottom 96-well plates (Greiner, Kremsmünster, Austria, #655090) at a density of 30,000 cells/well and incubated for at least at 24 h at 37 °C. Ca^{2+} flux assay was performed as described previously [27, 35]. In brief, cell culture medium was removed, cells were labeled with 100 µL/well of Fluo-2 AM dye solution (2.4 µM Fluo-2 AM, 0.06% (*v/v*) Pluronic-F127) in assay buffer (20 mM HEPES, 2.5 mM probenecid in HBSS, pH 7.5) and incubated for 60 min at 37 °C. Afterwards, the dye solution was replaced by 50 µL/well assay buffer and basal Ca^{2+} levels were detected for 20 s with a FlexStation III device (Molecular Devices, San Jose, CA, USA) using a fluorescent read-out (λ_{ex} = 485 nm, λ_{em} = 525 nm). After 20 s, 50 µL/well of DMSO control or 2× compound solution was automatically added and Ca^{2+} response was measured for 60 s. Following, 20 µL/well of 6× serially diluted ligand solution (for full curves) or a single PP EC_{30} concentration (for mutagenesis studies) was added. Ca^{2+} response was measured over a total run time of 140 s. Raw data were quantified as *x*-fold over basal. Normalization and calculation of nonlinear regression were performed with GraphPad Prism 9.0 (GraphPad Software, San Diego, CA, USA; RRID: SCR_002798). Allosteric parameters were

determined by using an operational model of allosterism (1) [36], whereas E describes the pharmacological effect, A and B are the concentration of the orthosteric and allosteric ligand, respectively, K_B and τ_B represent the equilibrium dissociation constant and the operational index of efficacy of the allosteric modulator, EC_{50} is the half-maximal molar concentration of the orthosteric ligand, $\alpha\beta$ is referred to as cooperativity factor, and E_m and n represent the maximal responsiveness of the system and the Hill slope, respectively.

$$E = Basal + \frac{(E_m - Basal)([A](K_B + \alpha\beta[B]) + \tau_B[B][EC_{50}])^n}{[EC_{50}]^n(K_B + [B])^n + ([A](K_B + \alpha\beta[B]) + \tau_B[B][EC_{50}])^n} \quad (1)$$

G protein sensor BRET

Direct G-protein activation was investigated in a BRET-based approach using G protein sensors [37]. Plasmids encoding native Y_4R (500 ng) and tricistronic G protein biosensor (500 ng) were co-transfected into 80% confluent COS-7 cells in 25 cm^2 cell culture flasks using Metafectene Pro transfection reagent, according to the manufacturer's protocol. To ensure Y_4R-specific G-protein activity, mock vector (pcDNA3 plasmid) was used as control instead of Y_4R plasmid. The day post transfection, cells were resuspended in phenol red-free DMEM/F-12 supplemented with 10% FBS, and reseeded into white solid 96-well plates at a density of 50,000 cells/well for another 24 h. Prior to BRET measurements, cell medium was replaced by 50 µL of BRET buffer (25 mM HEPES in HBSS, pH 7.4). After the addition of 50 µL of coelenterazine h (4.2 µM final concentration), cells were incubated for 5 min at 37 °C, following the addition of 50 µL of 4× concentrated compound solution (0.3–30 µM) for another 3 min at 37 °C. For endpoint measurements, cells were stimulated with 50 µL of varying PP concentrations (10^{-6} to 10^{-12} M final concentration) or buffer as control, and incubated for 20 min at 37 °C. Fluorescence (400–470 nm) and luminescence (535–600 nm) were measured well-wise with an integration time of 500 ms using a Tecan Spark plate reader (Tecan, Männerdorf, Switzerland). For kinetic measurements, fluorescence and luminescence were continuously recorded for 35 min at 37 °C in live COS-7 cells. After the addition of coelenterazine h and compound solution at different concentrations, the plate was placed in the plate reader and baseline was detected for 5 min, followed by the stimulation of the cells with 1 nM of PP final concentration. Raw BRET was calculated by dividing the fluorescence values by the luminescence values. NetBRET values were obtained by subtraction of the BRET values of the buffer control from stimulated values. For kinetic measurements, the netBRET values from the buffer control were additionally subtracted from the stimulated values at each time point of the measurement.

Live cell glosensor cAMP measurement

The activation of the endogenous Y_4R $G_{i/o}$ pathway in response to PP was monitored using Glosensor cAMP assay (Promega) in COS-7 cells, according to the manufacturer's protocol. In brief, COS-7 cells at a density of 70–80% were transiently co-transfected with $Y_{1/2/4/5}R$-eYFP and pGloSensor-22 F cAMP plasmid (ratio 1:1, endpoint measurement) or Y_4R-eYFP and the pGloSensor-22 F cAMP plasmid (ratio 1:1, kinetic measurement) overnight using Metafectene Pro transfection reagent. The following day, the cells were reseeded into white solid 384-well plates with a density of 15,000 cells (endpoint measurements) or white solid 96-well plates at a density of 50,000 cells per well (kinetic measurement) and incubated for 24 h under standard cell culture conditions. On the assay day, cell culture medium was aspirated and cells were equilibrated with 20 µL/well (endpoint measurements) or 100 µL/well (kinetic measurement) of a 2% (*v/v*) GloSensor cAMP reagent stock solution in buffer (HBSS with 25 mM HEPES) for 2 h at RT until a stable basal signal was obtained. For endpoint measurement, compound solutions (0.3, 1, 3, 5, 10, 20, and 30 µM of C1 final concentration), peptide dilutions (ranging from 1 pM to 10 µM final concentration) and forskolin (5 µM final concentration) were prepared in BRET buffer at RT. Following incubation, cells were treated with 5 µL/well of 8× compound solution or DMSO as control. After an incubation of 5 min, 5 µL/well of 8x peptide solution or buffer was added, and cells were incubated for additional 5 min. Subsequently, 10 µL/well of 4x forskolin solution was added. The luminescence signal was measured 20 min after addition of forskolin with an integration time of 500 ms using Tecan Spark plate reader. A non-linear regression was performed using GraphPad Prism 10.6.1 and curves were normalized to DMSO control. For kinetic measurement, compound solutions (0.3, 3, and 30 µM of C1 final concentration), peptide dilution (PP at a final concentration of 1 nM) and forskolin (10 µM final concentration) were prepared in BRET buffer at RT. Following incubation, cells were treated with 25 µL/well of 8× compound solution or DMSO as control. Subsequently, the plate was placed in a Tecan Spark plate reader and luminescence was recorded continuously over 45 min with an integration time of 500 ms. After 5 min, the run was paused, cells were stimulated with 50 µL/well of the agonist PP (1 nM, 4× concentrated), and after 10 min forskolin, a direct activator of the adenylyl cyclase, at a final concentration of 10 µM was added. For data evaluation, baseline values (only compound solution in buffer) were removed from each value. Data were normalized to the maximal DMSO control (100%) and baseline control (0%). GraphPad Prism 9.0 was used to plot luminescence signals over time.

Y_4R membrane preparation

Y_4R membranes were obtained from stably transfected HEK293_Y_4R-eYFP cells. At a confluency of about 90%, cells were harvested using DPBS and collected by centrifugation for 5 min at 1,800 rpm, 4 °C. The next steps were continuously performed on ice. The cell pellet was resuspended in ice-cold tris buffer (50 mM tris, 50 µM Pefabloc, pH 7.5) and homogenized using a Dounce homogenizer. The cell suspension was centrifuged for 20 min at 2,400 rpm, 4 °C. The obtained supernatant was carefully collected and centrifuged for 60 min at 12,000 rpm, 4 °C. The supernatant was discarded and the pellet containing membranes was resuspended in ice-cold HEPES buffer (25 mM HEPES, 25 mM $CaCl_2$, 1 mM $MgCl_2$, 50 µM Pefabloc, pH 7.4) and homogenized with a Dounce homogenizer. The suspension was again centrifuged for 60 min at 12,000 rpm, 4 °C. The supernatant solution was discarded, and the pellet was suspended in HEPES buffer. Protein concentration was determined using Bradford protein assay [38]. Aliquots of membrane preparations were stored at − 80 °C until use.

Radioligand binding assay

Radioligand binding experiments were performed using membrane preparations of stably transfected HEK293-hY_4R-eYFP cells, as described [27, 35]. In short, DMSO vehicle and C1 solutions were prepared in ice-cold HEPES buffer (25 mM HEPES, 2.5 mM $CaCl_2$, 1.0 mM $MgCl_2$, 1% BSA, 1% 5 mM Pefabloc) and 40 µL/well were added to a translucent non-binding 96-well plate (Greiner, #655901). Y_4R membrane preparations were gently thawed on ice, suspended in cold HEPES buffer, and added to the DMSO and C1 solutions (40 µL/well, final concentration 0.3 µg). ^{125}I-PP (human) or ^{125}I-PYY (human) peptide solutions were prepared in MilliQ water, supplemented with 1.0% BSA. Ten µL of 10× radiolabeld peptide solutions (30 pM ^{125}I-PP or 150 pM ^{125}I-PYY, final concentration) were added to Y_4R membranes. To determine unspecific binding, 10 µL of unlabled PP at a final concnetration of 1 µM was added instead of 10 µL of 1.0% BSA. Binding assays were incubated for 4 h at RT under gentle shaking until equilibrium has reached. Afterwards, Y_4R membrane-bound ^{125}I-PP or ^{125}I-PYY were separated by filtration with a GFC filter (PerkinElmer), presoaked with 0.1% polyethylenimine (*w/v*) in PBS using a MicroBeta Filtermat-96 Cell Harvester System (PerkinElmer). Membranes were washed three times with ice-cold PBS, dried for 15 min at 55 °C, and treated with MeltiLex solid scintillation sheets. Radioactivity of Y_4R-bound ^{125}I-PP or ^{125}I-PYY was measured using a MicroBeta 2 scintillation counter (PerkinElmer).

Arrestin BRET

Arrestin-3 recruitment to Y_4R was investigated by BRET assay in transiently transfected COS-7 cells, as described [27]. For transient transfection, COS-7 cells were grown in 75 cm^2 cell culture flasks to a density of about 80% and transfected with 1,000 ng Y_4R-Rluc8 and 11,000 ng Venus-arrestin-3 using Metafectene Pro, according to the manufacturer's protocol. The next day, cells were resuspended in phenol red-free DMEM/F-12 supplemented with 10% FBS, and seeded into white solid 96-well plates (Greiner, #655083) at a density of 50,000 cells/well. COS-7 cells were incubated for at least 24 h under standard conditions. For BRET measurements, cell medium was removed and 100 µL of BRET buffer (HBSS, 25 mM HEPES, pH 7.4) containing DMSO vehicle or a final concentration of 30 µM of C1 was added. For endpoint measurements, 50 µL of 4× serially diluted peptide ligand was added, followed by the addition of 50 µL of coelenterazine h at a final concentration of 4.2 µM. The plate was incubated for 5 min at 37 °C before measurement was performed with a Tecan Infinite M 200 Plate Reader (Tecan) using the filter sets GREEN1 (Venus fluorophore, 520–570 nm) and BLUE1 (Rluc8, 370–480 nm). For kinetic studies, 50 µL of coelenterazine h (4.2 µM final concentration) was added, and baseline was measured for 5 min in the plate reader. Afterwards, cells were subsequently stimulated with agonist or blank (BRET buffer), and BRET signals were measured continuously over 30 min at 37 °C in a Tecan Infinite M 200 Plate Reader. BRET signals were calculated as the ratio of fluorescence divided by luminescence. netBRET signals were obtained by the subtraction of the BRET ratio of unstimulated cells from stimulated cells.

Data analysis and statistics

Calculations of mean, SEM, and nonlinear regression were performed using the statistics program GraphPad Prism 9.0 and 10 (GraphPad Software, San Diego, CA, USA; RRID: SCR_002798). For statistical analysis, unpaired t-test, or one-way ANOVA with Dunnett's multiple comparison post test was applied. Data are expressed as mean ± SEM. The applied statistical tests and exact sample sizes are given in the respective Figure legends.

Optimization of the PP-Y_4R cryo-EM structure

The PP-Y_4R optimized complex structure were generated as described previously [39]. Only the atom coordinates of the PP-Y_4R complex were extracted from the cryo-EM structure (PDB ID: 7X9C) [7]. The atom names of the N-terminal

amidated tyrosine residue of PP was manually changed to match with Rosetta's naming convention. The PP-Y_4R complex structure was then relaxed with constraints to the starting structures [40]. The 100 output relaxed models were used as templates for the FlexPepDock refinement peptide docking protocol [41] to generate 3,000 output models. The top 30 docking models with the best interface interaction scores were selected to be the templates for the next step of ligand docking.

Induced-fit docking of C1 to the optimized of PP-Y_4R cryo-EM structure

A set of 100 conformations of C1 was generated using the ConformerGenerator application of BCL::Conf [42–44]. This application builds small-molecule conformations from substructures derived from small molecule crystal structures in the Crystallography Open Database (COD; RRID: SCR_005874). RosettaLigand (Rosetta 3.12; RRID: SCR_015701) [45, 46] was used to dock C1 to PP-Y_4R models. A starting position was selected for C1 based on the proximity to residues that are important to C1 activity according to mutagenesis data. The induced-fit docking protocol started with an initial docking round that allows the ligands conformation sampling as well as rotation and translation. The docking protocol included a low resolution (centroid mode) phase consisting of 500 cycles sampling ligand conformers in 4 Å translation search and complete reorientation search, and a high-resolution phase consisting of six cycles of sidechain refinement with small perturbations of ligand poses and conformation. Throughout the conformation sampling process, constraints were set so that the ligand would not move too far from the initial placement. Then, another round of relaxing the backbone of the residues surrounding the ligand to mimic the induced fit effect, and a final refinement docking to optimize the ligand-receptor atomic interactions was performed [40]. During the refinement phase, the translation search was reduced to 1 Å. This phase finds an energetically favorable pose by combining minor ligand conformational flexibility with sidechain refinement simultaneously. The top 5% output models by interface delta score were collected, then clustered into 3 clusters. The Rosetta interface scores versus ligand RMSDs graphs after the final round of induced fit docking are shown in Fig. S7.

Mutagenesis agreement score computation on output docking clusters

For each of the three clusters, the mutagenesis agreement score was computed such that the scores are higher when an important residue (according to mutagenesis data) has favorable binding energy toward the ligand. The mutagenesis agreement score of a cluster t is calculated as mutagenesis agreement score (t) = - ∑PRIEi, where PRIEi is the predicted per-residue interaction energy between the ligand and an important residue. Mutagenesis agreement scores for all three clusters are listed in the Supplementary Table S2.

Gain-of-function Y_4R mutant prediction

For each cluster, the top 10 models were used as template models for the calculations. The residues that interact with C1 were redesigned with the Rosetta binding pocket design protocol [47]. Only one residue was allowed to mutate during each run. Only the output Y_4R mutants that showed improvement in interface scores were selected.

Results

Identification of C1 as Y_4R PAM at the G-protein signaling pathway

Following a HTS campaign of 81,600 compounds from the Vanderbilt Discovery Collection, a drug-like custom library, C1 (Fig. 1A) was identified as novel PAM at Y_4R with a hit rate of PAMs of 0.015%. To consider the structural importance of the ethyl acetate moiety of the hit compound C1, a structural analog lacking this side chain was included in the study (C2, Fig. 1A). To monitor the effect of both compounds on G-protein activation in response to the endogenous peptide agonist PP, we first used Y_4R-mediated Ca^{2+} flux assay in stably transfected COS-7_hY_4R-eYFP_$\Delta 6G\alpha_{qi4-myr}$ cells. Titration of the small molecules C1 and C2 induced a concentration-dependent potentiation of the native agonist PP response compared to DMSO vehicle, reaching a saturable effect at 3 µM for C1 and 30 µM for C2 (Fig. 1B). The functional data were analyzed with an operational model of allosterism by Aurelio et al. [36]. to quantitatively assess modulator affinity (K_B), functional cooperativity (αβ), and allosteric agonism (τ_B) between both compounds. C1 showed an affinity of 790 nM (pK_B ± SEM: 6.1 ± 0.18) to Y_4R, whereas binding affinity of C2 was reduced by more than 10-fold compared to C1 with a K_B value of 8.5 µM (pK_B ± SEM: 5.1 ± 0.22). The positive cooperativity factor αβ indicates that the compounds enhance the ability of PP to promote Y_4R-mediated G-protein activation, but with a higher effect observed for C1 (αβ = 4.8) than for C2 (αβ = 3.5). These data highlight the structural importance of the ethyl acetate moiety for PAM activity on the Y_4R G-protein pathway, as both affinity and cooperativity were reduced for C2. The low τ_B values of 0.18 and 0.03 calculated for C1 and C2, respectively, indicate the absence of an intrinsic

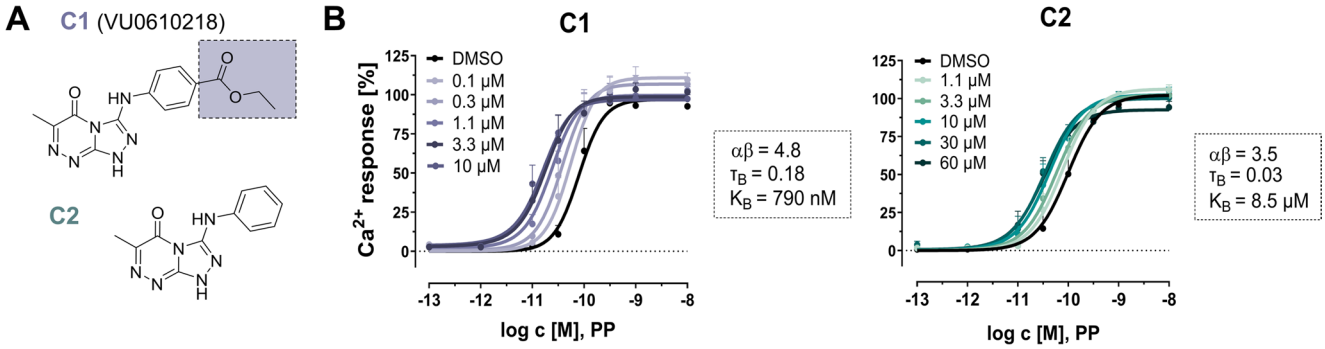


Fig. 1 C1 and C2 potentiate Y_4R G-protein signaling studied by Ca^{2+} flux assay. (**A**) Structure of C1 and C2 with the additional ethyl acetate moiety of C1 highlighted in lilac. (**B**) Titration of increasing concentrations of C1 and C2 induce a concentration-dependent leftward-shift of PP concentration-response curves compared to the DMSO control. Data were obtained by Ca^{2+} flux assay in COS-7_hY_4R-eYFP_Δ6G$\alpha_{qi4\text{-}myr}$ cells. The effects of C1 (> 1 µM) and C2 (> 10 µM) are saturable, indicating allosteric behavior. Data were fitted to an operational model of allosterism to calculate allosteric parameters: K_B – allosteric binding affinity, τ_B – intrinsic agonism, and αβ – allosteric cooperativity factor [36]

compound agonism (Fig. 1B) and confirm a pure PAM activity profile at Y_4R (Fig. S1).

Probe dependency and receptor selectivity of Y_4R PAMs

Next, receptor and ligand selectivity of the compounds was examined, as the Y_4R belongs to a complex multiligand/multireceptor system comprising four GPCRs (Y_1R, Y_2R, Y_4R, Y_5R) and three peptide ligands (NPY, PYY, PP). To investigate NPY- or PYY-mediated Y_4R activation, a saturating concentration of each compound (10 µM for C1 and 30 µM for C2) was used. Both compounds potentiate NPY- and PYY-mediated Y_4R activity compared to the DMSO control, indicated by the leftward-shift of the curves in the presence of the compounds (Fig. 2A). Statistical evaluation revealed a significant effect for C2 on NPY-mediated Y_4R signaling, while C1 exhibited a modest effect for NPY, notably weaker compared to the primary agonist PP. In contrast, PYY-induced G-protein activation at Y_4R was significantly enhanced by C1 and C2 with EC_{50} shifts by about 3-fold. Next, the subtype selectivity of C1 and C2 among Y_1R, Y_2R, and Y_5R was investigated by monitoring the receptor-mediated Ca^{2+} flux in COS-7 cells, stably expressing one specific receptor subtype. NPY was used as the endogenous, high-affinity ligand on these receptors. As indicated in Fig. 2B, C1 and C2 did not affect NPY-mediated G-protein signaling at Y_1R, Y_2R, and Y_5R compared to the DMSO vehicle when used at a maximal concentration of 30 µM. This indicates a high functional selectivity of C1 and C2 for the Y_4R subtype, as depicted in the radar plot for Y receptor selectivity (Fig. 2B), calculated as $\Delta\log(E_{max}/EC_{50})$ values [48].

In conclusion, we identified two PAMs that selectively potentiate Y_4R G-protein signaling with the highest effect observed for the ligand PP. C1 showed a significantly enhanced PAM activity at Y_4R compared to C2, highlighting the importance of its ethyl acetate moiety for PAM activity and affinity. Thus, only C1 was used for further characterization.

C1 affects Y_4R G-protein activity in G protein BRET and cAMP assays

To further evaluate the effect of the PAM C1 at Y_4R on its native $G_{i/o}$ pathway and to exclude effects due to the chimeric G protein, two additional assays were used: G protein sensor BRET [37], which allows the direct measurement of $G_{i/o}$ protein activity by monitoring the dissociation of the Gα and Gβγ moiety (Fig. 3A), and GloSensor cAMP assay [49], which uses a biosensor to monitor the intracellular second messenger cAMP in response to the activation of the Y_4R-coupled $G_{i/o}$ pathway. In kinetic G protein BRET assays using the G_{i3} sensor, C1 potentiated the PP-mediated Y_4R G-protein activation as demonstrated by the reduction of the netBRET ratio in a concentration-dependent manner upon stimulation with a half-maximal concentration of PP (1 nM) over 30 min (Fig. 3B). Comparison of the $BRET_{max}$ ratios indicate a significant increase in presence of the PAM, which is associated with an enhanced G-protein activity. In endpoint measurements, we have shown that C1 slightly, but not significantly, improves PP potency (leftward-shift of curves), but markedly increased the efficacy ($BRET_{max}$) in G-protein dissociation for PP in a concentration-dependent manner compared to the DMSO control (Fig. 3C) using two different G protein sensors, G_{i3} and G_{o1} (Fig. S2). Thus, the data highlight an improved G-protein coupling in the presence of the PAM.

To clarify how C1 acts further downstream on the native G_i signaling pathway, GloSensor cAMP assay has been used.

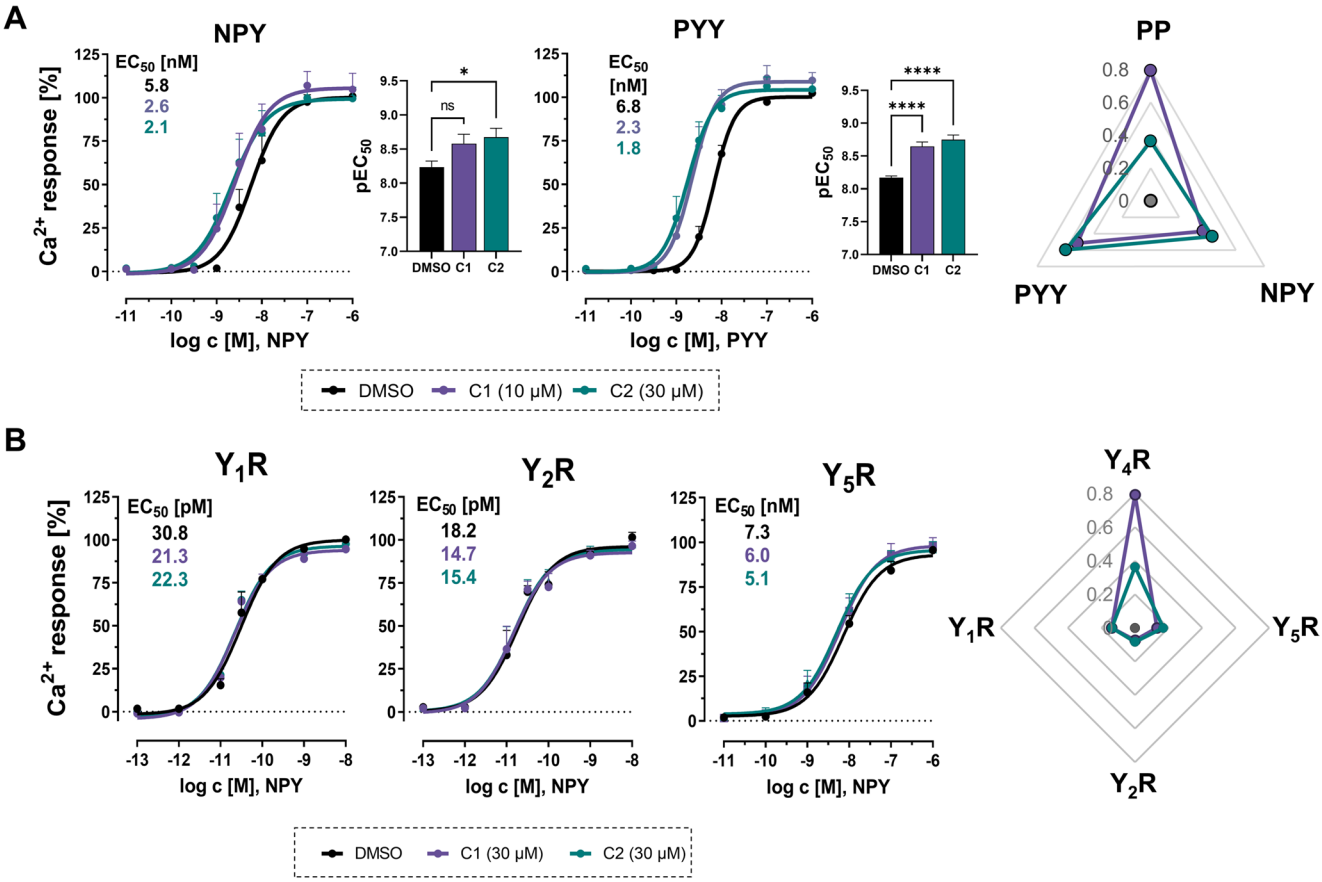


Fig. 2 The PAMs C1 and C2 show a Y_4R-selective potentiation of G-protein signaling independent of the peptide agonist. (**A**) Probe dependence effects of the compounds. Potentiation of Y_4R G-protein signaling in the presence of 10 µM of C1 and 30 µM of C2 in response to the low-affinity ligands NPY and PYY. DMSO was used as control. Ca^{2+} flux assays were performed in COS-7_hY_4R-eYFP_$\Delta 6G\alpha_{qi4\text{-}myr}$ cells. Statistical significance was determined by one-way ANOVA and Dunnett's post test; ns, not significant; *, $P < 0.05$; ****, $P < 0.0001$. Radar plot illustration on ligand selectivity for the PAMs C1 and C2, shown as $\Delta\log(E_{max}/EC_{50})$ values based on data from Ca^{2+} flux experiments. (**B**) Effect of 30 µM of C1 or C2 on Y_1R, Y_2R, and Y_5R G-protein activation. Y receptor selectivity was investigated in COS-7 cells stably co-expressing Y_1R, Y_2R, or Y_5R, C-terminally fused to eYFP, and the chimeric G protein $\Delta 6G\alpha_{qi4\text{-}myr}$. Radar plot presentation on Y receptor selectivity for the PAMs C1 and C2, shown as $\Delta\log(E_{max}/EC_{50})$ values based on NPY-activation data from Ca^{2+} flux experiments. Data are shown as mean ± SEM from $N \geq 3$ independent experiments. Radar plots have been generated based on [48]

For this purpose, the basal cAMP level of Y_4R-expressing COS-7 cells was studied using the adenylyl cyclase activator forskolin. As shown in the concentration-response curve, increasing concentrations of PP lead to a reduction of Y_4R-mediated cAMP levels (Fig. 4A, left). Notably, co-stimulation with increasing concentrations of C1 did not produce a leftward-shift of the concentration-response curve of PP at Y_4R, but instead reduces the basal cAMP level (Fig. 4B), suggesting that C1 may also enhance the constitutive activity of Y_4R [50]. In line with the Ca^{2+}flux assay, this effect was not observed at Y_1R, Y_2R, or Y_5R using a high concentration of C1, indicating a subtype-selective activity of C1 at Y_4R (Fig. 4B). Additionally, we performed kinetic cAMP measurements at Y_4R. Here, 10 µM of the adenylyl cyclase activator forskolin increases the intracellular cAMP levels in Y_4R-expressing COS-7 cells. Stimulation with the peptide agonist PP (1 nM) in the presence of 0.3% DMSO reduced intracellular cAMP levels compared to the forskolin control, demonstrating G_i activation (Fig. 4C, left). To test the effect of the PAM C1 on a kinetic level, cells were stimulated with two concentrations of C1 (3 and 30 µM) or DMSO as control for 5 min. Afterwards, cells were stimulated with PP for another 5 min, before forskolin was added to increase intracellular cAMP levels. Compared to the DMSO control, C1 reduced the relative cAMP response, confirming the potentiation of PP-induced G_i signaling of Y_4R (Fig. 4C, right). This effect saturated at low concentrations of C1, pointing towards a markedly higher inhibition of the adenylyl cyclase activity over time. These studies confirmed the PAM effect of C1 at Y_4R on the native G_i pathway using G protein BRET as a direct read-out for G-protein activity, as well as in the second messenger cAMP assay.

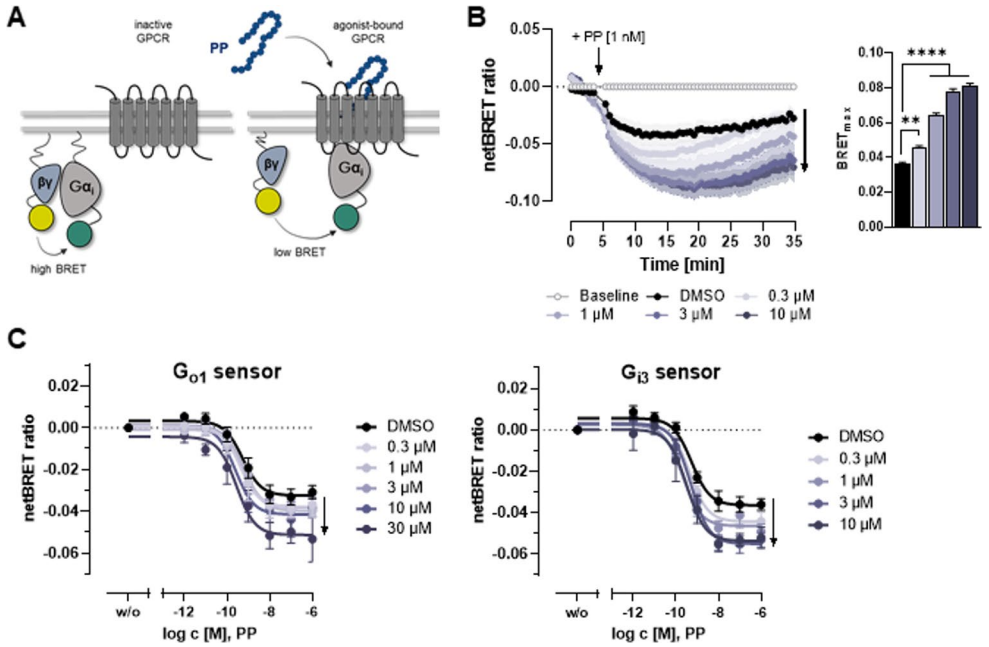


Fig. 3 C1 potentiates native Y_4R-mediated $G_{i/o}$ signaling. (**A**) Assay principle of G protein BRET sensors according to Schihada et al. [37]. (**B**) Kinetic G protein BRET measurements using the G_{i3} BRET sensor. Y_4R-mediated G-protein activity was detected in the presence of different concentrations of the PAM C1 and initiated by the addition of 1 nM of the agonist PP after about 5 min of baseline detection. $BRET_{max}$ values are summarized as bar graphs. Statistical analysis was performed using one-way ANOVA with Dunnett's post test, **, $P < 0.01$; ****, $P < 0.0001$. (**C**) Endpoint measurements of G-protein activity after 30 min of ligand stimulation using G_{o1} or G_{i3} BRET sensors in the presence of DMSO or different concentrations of C1. C1 increases the $BRET_{max}$ of PP concentration-response curves compared to the DMSO control, indicated by black arrows. G protein BRET assays were conducted in COS-7 cells transiently co-transfected with Y_4R and the respective G protein sensor. Data are shown as mean ± SEM from $N \geq 3$ independent experiments

C1 slightly increases the affinity of the agonists PP and PYY to the Y_4R orthosteric site

The presence of allosteric modulators has been shown to affect the conformational landscape of its cognate receptor, which can modulate the affinity and binding mode of the orthosteric agonist. Therefore, the effect of C1 on the affinity of the peptide ligands PP and PYY to Y_4R membrane preparations was investigated by radioligand binding assay using ^{125}I-PP and ^{125}I-PYY. Y_4R membranes were incubated with C1 and the radioligand for about 4 h until equilibrium was reached. C1 slightly enhanced the binding of ^{125}I-PP to Y_4R membranes for concentrations up to 10 µM compared to the DMSO control, while this effect was not observed at the highest concentration of 30 µM (Fig. 5A). A similar effect of C1 was observed for the binding of ^{125}I-PYY to Y_4R membranes at equilibrium (Fig. 5B). Here, C1 increased the affinity of ^{125}I-PYY to Y_4R up to a concentration of 3 µM, whereas binding of PYY was unaffected at high compound concentrations (10 µM and 30 µM).

Effect of C1 on arrestin-3 recruitment to Y_4R

The Y_4R was previously observed to recruit arrestin-3 after agonist stimulation [51]. Therefore, we assessed the effect of C1 on the arrestin-3 recruitment pathway in addition to G-protein signaling. The Y_4R-arrestin-3 interaction was studied by BRET assay in COS-7 cells transiently expressing Y_4R-*Renilla* luciferase 8 (Rluc8) and Venus-tagged arrestin-3 using two different set-ups: kinetic measurements, at which PP-induced arrestin-3 recruitment was constantly detected over 30 min, and endpoint measurements, at which arrestin-3 recruitment was detected 5 min after stimulation with increasing PP concentrations. In kinetic experiments, treatment of COS-7 cells with 30 µM of C1 induced a significant increase in the maximal netBRET ratio of arrestin-3 recruitment to Y_4R compared to DMSO after stimulation with 100 nM of the agonist PP. Arrestin-3 was mainly recruited to Y_4R within the first 10 min after PP stimulation and started to dissociate from the receptor shortly afterwards (Fig. 5C). Therefore, BRET signals from concentration-dependent measurements were detected after 5 min of agonist stimulation. Compared to DMSO, we observed a significant enhancement of the efficacy (E_{max}) in arrestin-3 recruitment in the presence of high concentrations of C1 (30 µM) by about 20%, while potency of arrestin to Y_4R remained unaffected in the presence of C1 with an EC_{50} value of 4.2 nM (pEC_{50} ± SEM: 8.38 ± 0.09) (Fig. 5D). This suggests a positive allosteric effect of C1 in the arrestin-3 recruitment pathway.

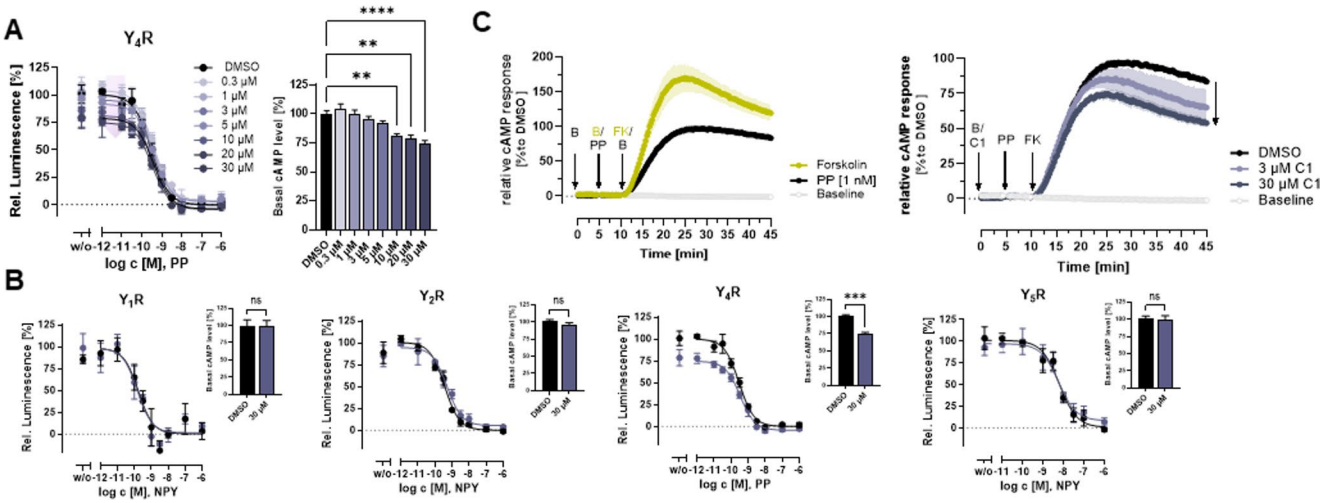


Fig. 4 C1 selectively modulates basal Y_4R activity. (**A**) Endpoint measurement of Y_4R activity in cAMP GloSensor assay in COS-7 cells transiently expressing Y_4R-eYFP and the GloSensor-22 F plasmid after 20 min of ligand stimulation in the presence of DMSO or different concentrations of C1. The basal cAMP levels relative to DMSO control was obtained from non-linear regression and are summarized as bar graphs. Statistical analysis was performed using one-way ANOVA with Dunnett's post test, **, $P<0.01$; ****, $P<0.0001$. (**B**) Endpoint measurement of Y receptor activity in cAMP GloSensor assay in COS-7 cells transiently expressing Y_1R, Y_2R, Y_4R, or Y_5R and the GloSensor-22 F plasmid after 20 min of ligand stimulation in the presence of DMSO or 30 µM of C1. The basal cAMP levels relative to DMSO control was obtained from non-linear regression and are summarized as bar graph. Statistical analysis was performed using unpaired t-test, ns, not significant; ***, $P<0.001$. (**C**) Time-dependent GloSensor cAMP assay in COS-7 cells transiently expressing Y_4R-eYFP and the pGloSensor-22 F cAMP plasmid for investigating the native Y_4R-mediated $G_{i/o}$ protein signaling pathway. Cells were stimulated with DMSO or C1 subsequently before the measurement. The agonist PP or buffer (B, as control) were added after 5 min of baseline detection. Adenylyl cyclase activity was stimulated by the addition of 10 µM of forskolin (FK) after about 10 min. Luminescence was continuously monitored over 40 min and relative cAMP response was normalized to DMSO control. C1 reduces relative cAMP response compared to DMSO, indicated by the black arrow. Data are shown as mean from $N\geq3$ independent experiment; SEM is shown as shaded bands

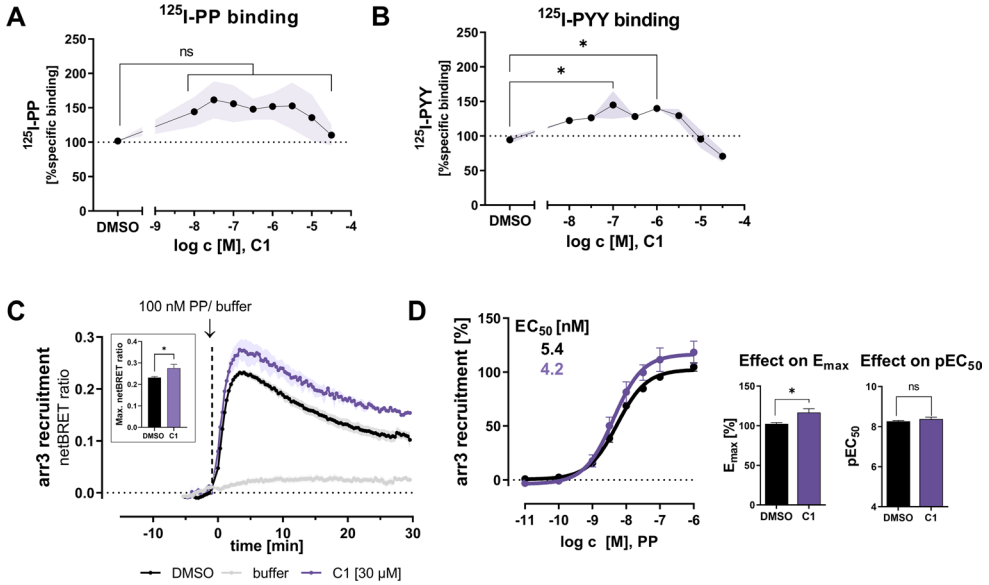


Fig. 5 C1 slightly enhances ligand affinity and arrestin-3 recruitment to Y_4R. (**A**, **B**) Effect of increasing concentrations of C1 on the binding of 30 pM ^{125}I-PP (A) or 150 pM ^{125}I-PYY (B) to membrane preparations from HEK293 cells stably expressing Y_4R. Data represent the mean from $N\geq3$ independent experiments, SEM are shown as shaded bands. Statistical significance was determined by one-way ANOVA with Dunnett's post test; ns, not significant; *, $P<0.05$. (**C**, **D**) BRET analysis was used to study the effect of 30 µM of C1 on arrestin-3 recruitment to Y_4R using COS-7 cells, transiently expressing Y_4R-Rluc8 and Venus-arrestin-3. Arrestin-3 recruitment kinetics were monitored over 30 min after stimulation of the receptor with 100 nM of the agonist PP. Data represent the mean from $N\geq2$ independent experiments, SEM are shown as shaded bands (C). Effect of 30 µM of C1 on PP concentration-response curves was measured after 5 min of agonist stimulation. DMSO is used as control. Data are shown as mean ± SEM from $N\geq3$ independent experiments (D). Statistical evaluation was performed using unpaired student's t-test, ns, not significant; *, $P<0.05$

Identification of a potential binding mode of C1 at Y_4R obtained by mutagenesis and computational docking

To better understand the effect of C1 on PP modulation, we characterized the potential binding pocket of C1 to Y_4R by mutagenesis and computational docking. To get a first hint on Y_4R segments that are important for the PAM effect of C1, different Y_4R/Y_1R chimeric receptors were used. The PAM effect was studied as the relative potentiation of a low-efficacy PP concentration (PP EC_{30}) at each chimera in a Ca^{2+} flux-based assay set-up using COS-7 cells transiently expressing a chimeric receptor variant and the G protein chimera $\Delta 6G\alpha_{qi4-myr}$.

Y_4R/Y_1R chimeras highlight the relevance of residues within transmembrane (TM) helix 1, TM2, extracellular loop 1 (ECL1), TM6, and TM7 of Y_4R for C1 activity

The use of Y_4R/Y_1R chimeras allows the identification of relevant receptor segments and amino acid residues differing between the Y_1R and Y_4R subtype. Here, we investigated the effect of C1 (10 and 30 µM) on the potentiation of the PP EC_{30} response at seven different Y_4R/Y_1R chimeras (Fig. 6A, Table S1). The absolute potentiation of PP response induced by 10 µM of C1 versus DMSO is illustrated as bar graphs (Fig. 6B). At Y_4R WT, C1 induced a relative potentiation of the PP EC_{30} response by 23% in transiently transfected COS-7 cells. The C-terminal exchange of Y_4R segments, ranging from intracellular loop 3 (ICL3) to the C terminus, indicates the involvement of some residues in the Y_4R regions TM6-ECL3-TM7 for C1 activity, as the PAM effect is slightly reduced at this chimera (chimera B; Fig. 6). The exchange of a large Y_4R segment, covering the N terminus up to the end of TM5 by the corresponding Y_1R sequence, resulted in a significant loss of PAM activity, and highlights the importance of the N-terminal region for the PAM activity of C1 (chimera C; Fig. 6). Next, Y_4R/Y_1R chimeras with smaller segmental exchanges at the N-terminal receptor part were studied (chimera D and E; Fig. 6). At chimera D, in which the N terminus and TM1 of Y_4R are replaced by the corresponding sequence of Y_1R, a complete loss of PAM activity was found for C1. Thus, TM1 seems to be strongly involved in the interaction with the compound. The replacement of ICL1 and TM2 of Y_4R resulted in a moderate loss of PAM activity with a remaining potentiation of about 11% (chimera E; Fig. 6). Next, Y_4R loop chimeras were investigated. Chimera F contains a replacement of the Y_4R ECL1 by the loop of the Y_1R. This exchange led to a significant loss of C1 activity by about 10-fold, indicating the relevance of residues within ECL1 for C1 activity. The exchange of the large ECL2 of Y_4R by the corresponding loop of the Y_1R revealed a relative potentiation of 22% comparable to the WT and is negligible for compound activity (chimera G; Fig. 6). The replacement of the ECL3 of Y_4R by the ECL3 of Y_1R did not exhibit a clear loss of C1 PAM activity with a potentiation of PP EC_{30} response to 17% (chimera H; Fig. 6). Thus, these data indicate that TM1, TM2, ECL1, TM6, and TM7 might contain relevant residues required for C1 PAM activity (Fig. 6C).

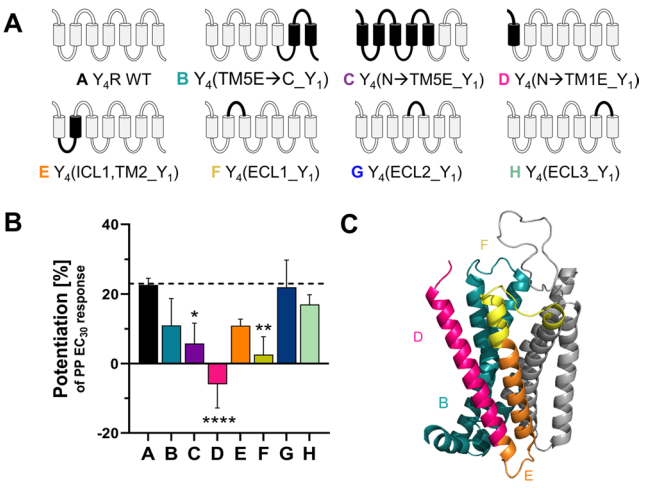


Fig. 6 Important Y_4R segments for C1 activity identified using Y_4R/Y_1R chimeras. (**A**) Schematic representation of Y_4R/Y_1R chimeras. Grey color represents Y_4R segments, Y_1R segments are colored in black. (**B**) Relative potentiation of the PP EC_{30} response in the presence of 10 µM of C1 compared to DMSO. Mutagenesis studies were performed using Ca^{2+} flux assay in transiently transfected COS-7 cells expressing one Y_4R/Y_1R chimera and the chimeric G protein $\Delta 6G\alpha_{qi4-myr}$. Data are shown as mean ± SEM from $N \geq 3$ independent experiments. Statistical significance was determined by one-way ANOVA with Dunnett's post test; *, $P<0.05$; **, $P<0.01$; ****, $P<0.0001$. (**C**) Highlighting of important Y_4R segments according to the mutagenesis studies using Y_4R/Y_1R chimeras (PDB: 7X9C)

Single-point mutagenesis in combination with computational docking revealed potential binding poses of C1 at Y_4R

Single point mutagenesis identified important Y_4R residues for PAM activity

To identify specific Y_4R positions involved in the interaction with C1, a mutagenesis scan of Y_4R positions located at the extracellular interface was performed. Here, the effect of 10 µM and 30 µM of C1 on the potentiation of the PP EC_{30} response at 41 Y_4R variants was investigated by Ca^{2+} flux assay (Table S1). For the screen, Y_4R residues that are known to be important for the endogenous peptide ligand PP or a reported Y_4R allosteric antagonist have been included [7, 35]. At Y_4R WT, C1 induced a relative potentiation of the PP EC_{30} response by about 25% in the presence of 10

µM and 30 µM of C1 (Table S1). As shown for Y_4R/Y_1R chimeric receptors, TM1, TM2 and ECL1 have been shown to be important receptor domains for C1 activity. A deeper insight into these regions revealed that Ala mutations of Y1.39, Q2.58, L2.60, and T2.61, as well replacements of the regions 1.26–1.28 and 1.37–1.38 by Y_1R residues significantly reduced the PAM activity of C1, while mutations of the residues 1.30–1.33, 1.40–1.43, M2.53, Y2.64 and W2.70 only resulted in a moderate loss of C1 activity. (Table S1, Fig. 7A). Mutation of residues 1.34–1.36 by the corresponding residues of Y_1R (Thr-Leu-Ala) induced an increase in C1 activity with a potentiation of PP EC_{30} response by 38% (Table S1, Fig. 7A). In TM3, mutation of S3.28 and C3.33 affected C1 activity with less than 10% PAM activity, while the variants S3.35 A and V3.36 A only moderately affect C1 activity. In TM5, residue L5.42 exhibited a clear loss in C1 activity if mutated to Ala (Table S1, Fig. 7). As indicated in Fig. 6, TM6 and TM7 are important receptor domains for C1 activity. Due to the sequence similarity of Y_4R and Y_1R within TM6 and TM7 (Fig. S3), identical residues between both subtypes were tested individually by single amino acid mutagenesis. Here, the Y_4R residues H6.52, D6.59, W6.60, and M7.43 were identified as important amino acids for C1 activity if mutated to Ala with less than 10% remaining PAM activity (Table S1, Fig. 7A, B). Y_4R residues without a clear effect on C1 potentiation are summarized in Table S1. Y_4R residues important for C1 PAM activity according to mutagenesis are visualized in Fig. 7C and reveal two potential binding pockets of C1. *Pocket I* is located within the Y_4R TM helical bundle and formed by residues within TM1, TM2, and TM7. The second cluster (*Pocket II)* is located between TM3, TM5 and TM6, however, in this cluster most

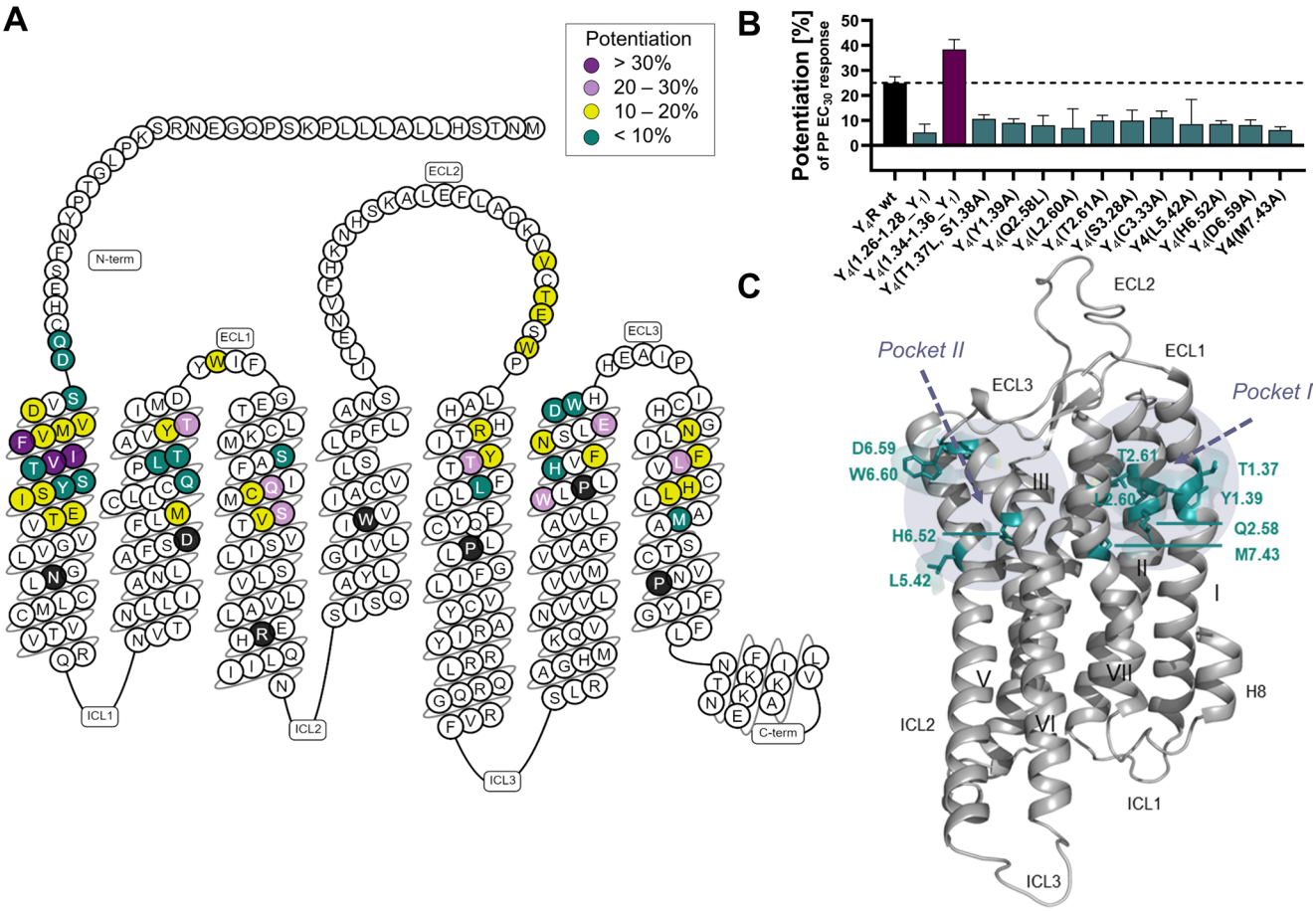


Fig. 7 Y_4R residues important for C1 activity investigated by mutagenesis. (**A**) Snake plot of Y_4R highlighting the tested residues for C1 PAM activity (adapted from GPCRdb.org). The color code represents the potentiation of the PP EC_{30} response at Y_4R variants in the presence of 30 µM of C1 investigated by Ca^{2+} flux assay: potentiation > 30% (dark purple), 20 – 30% (lilac), 10 – 20% (yellow), < 10% (cyan). Residues shown in black represent the most conserved residue per helix (x.50) according to the Ballesteros-Weinstein nomenclature. [52] (**B**) Relative potentiation of the PP EC_{30} response in the presence of 30 µM of C1 at the most important Y_4R variants. Mutagenesis studies were performed by using Ca^{2+} flux assay in transiently transfected COS-7 cells expressing a Y_4R variant and the chimeric G protein $\Delta 6G\alpha_{qi4\text{-}myr}$. Data are shown as mean ± SEM from $N \geq 3$ independent experiments. (**C**) Structural model of Y_4R (PDB: 7X9C) highlighting residues important for C1 PAM activity. Y_4R is shown in cartoon representation (grey), relevant residues with a loss of PAM activity are presented as cyan sticks. Two potential binding pockets according to mutagenesis are highlighted in light lilac, *Pocket I* and *Pocket II*

residues are pointing outside the binding pocket, making this pocket improbable.

Computational docking verifies binding to an Y_4R allosteric pocket

To obtain a more precise understanding on the binding mode of C1 at Y_4R, computationally induced-fit docking of the compound into an optimized Y_4R-PP cryo-EM structure (PDB: 7X9C) [7] was performed based on the mutagenesis data. Here, three potential binding clusters of the compound at Y_4R have been obtained. In all clusters, the PAM is placed in the core of the Y_4R 7-transmembrane (7TM) bundle near the C-terminal binding interface of PP, in a pocket mainly formed by residues in TM1, TM2, and TM7 (Fig. 8A). Thus, the molecular docking supports a binding of C1 in *Pocket I* (Fig. 7C), as suggested by mutagenesis. In cluster 0 and cluster 2, C1 occupies a similar allosteric pocket, while the compound in cluster 1 is located deeper within the helical bundle (Fig. 8A). Fig. 7B – D show the polar receptor and ligand environment of the compound in the three different clusters.

In cluster 0, the ethyl benzoate moiety of the compound is located in a crevice formed by TM1, TM2, and TM7. The ethyl acetate side chain of C1 points towards TM1 and TM2 of Y_4R and is engaged in a polar interaction with Q2.58 of Y_4R. Therefore, removal of the ethyl acetate side chain in C2 might destabilize the binding by the loss of a strong polar contact, which is indicated by a reduced affinity of C2 compared to C1. The triazine derivatives of C1 are orientated between TM2 and TM7 near the C terminus of the endogenous peptide ligand PP. Here, the aromatic heterocycle backbone is involved in polar interactions with R^{33} of PP and the Y_4R residues T2.65 and T2.61 in TM2 (Fig. 8B). Based on the mutagenesis data, mutation of the residues T2.61 and Q2.58 resulted in a severe loss of PAM activity, while the variant T2.65A shows no effect on the PAM effect, indicating no relevance of this residue for C1 activity (Fig. 7, Table S1).

In cluster 1, C1 forms a U-shaped conformation and is located deeper within the 7TM helical bundle compared to cluster 0 and 2. Here, the ethyl acetate side chain is oriented between TM1 and TM7 in a polar pocket formed by residues T1.43, C2.54, C7.47, and T7.46. The aromatic heterocycles are located deep inside the bundle in a cavity shaped by residues within TM2, TM3, and TM7 (Fig. 8A, C). Here, the nitrogen atoms of the triazole form direct polar interactions with the Y_4R residues T2.61, Q3.32, and H7.39. While mutation of position T2.61 to Ala markedly reduced the potentiation of PP-mediated Y_4R G-protein signaling, mutation of the polar residue Q3.32 had no effect on C1 activity (Fig. 7A, B). In cluster 1, C1 is in close proximity to the very C terminus of PP (Y^{36}-amide) highlighting the deep binding mode of the compound in this cluster (Fig. 8C).

In cluster 2, C1 binds within the 7TM helix bundle and is located in a similar pocket than the compound in cluster 0, but with a reversal orientation. Here, the ethyl benzoate group of C1 points up towards the extracellular receptor region and is located parallel to the C terminus of the endogenous agonist PP, which might allow the compound to form potential backbone interactions with the peptide agonist PP (T^{32}/N^{28}). Removal of the ethyl acetate as in C2 could therefore destabilize the PP-bound conformation and reduce the allosteric cooperativity with PP, which might explain the reduced PAM activity of C2 compared to C1 at Y_4R (Fig. 1). Additionally, C1 might form weak hydrophobic interactions with P^{34} of PP, further stabilizing the active conformation. In this cluster, the heterocycles of C1 are positioned between TM1, TM2, and TM7 and are engaged in a polar interaction network with residues S1.38, T2.61, and Q2.58 (Fig. 8D). Mutation of positions T2.61 and Q2.58 to Ala or Leu, respectively, resulted in a remarkable loss of PAM activity, indicating the importance of the polar residues for C1 activity. Position S1.38 showed a reduction of PAM activity by more than 60% in the double-mutated variant Y_4(T1.37L, S1.38A), highlighting the significance of the polar Y_4R residues for binding of C1 in cluster 2. Similar as in cluster 1, residue H7.39 forms a polar interaction with the nitrogen of the triazol ring of C1. With regard to the mutagenesis data, this position seems to be of minor relevance for C1 with about 70% remaining PAM activity of the Ala variant compared to the WT, while a mutation to Pro reduced the PAM activity by more than 50% (Fig. 7A, Table S1). This might indicate that the introduction of Pro might change the orientation of the helix by inducing a kink, and thus hampers important nearby interactions.

Based on these data, binding of C1 to Y_4R in cluster 2 is most likely as it fits well with mutagenesis data and shows the highest mutagenesis agreement score based on interface energy calculations (Table S2), while binding in cluster 1 is improbable.

Loss- and *gain-of-function* variants support the binding mode of C1 to Y_4R in cluster 2

To further verify the most likely binding mode of C1 to Y_4R, Y_4R residues that are in close proximity to the compound and might positively affect C1 activity have been predicted. To functionally evaluate the predicted variants, 14 Y_4R mutants have been created using single-point mutagenesis PCR and tested for G-protein signaling and membrane expression (Fig. S4). To obtain insight into the functional

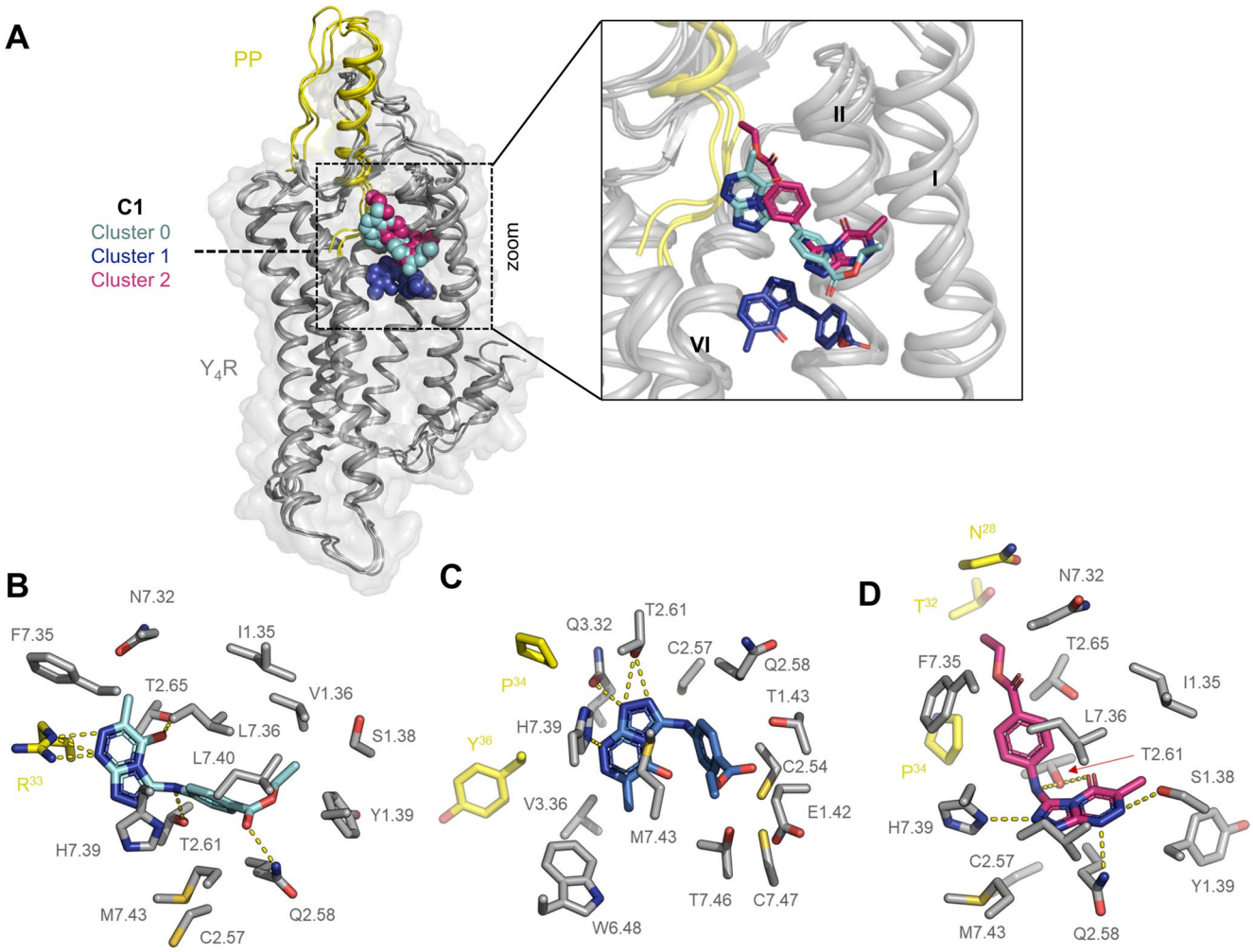


Fig. 8 Proposed binding poses of C1 to Y_4R in three clusters within the 7TM bundle. (**A**) Overlay of C1 binding clusters at Y_4R. Y_4R and PP are shown in cartoon representation in grey and yellow, respectively. TM7 is omitted for better illustration. C1 is shown as cyan (cluster 0), blue (cluster 1), or pink (cluster 2) spheres/sticks. For Rosetta docking, the PP-Y_4R-G_{i1} cryo-EM structure (PDB: 7X9C) was used as template for an optimized PP-Y_4R structure [7]. (**B-D**) Polar environment of C1 in cluster 0 (B), cluster 1 (C), and cluster 2 (D). Dashed yellow lines represent polar interactions between Y_4R residues (grey sticks) and C1 (cyan, blue, pink sticks). PP residues in the polar surrounding of C1 are shown as yellow sticks. Receptor residues are designated according to the nomenclature of Ballesteros-Weinstein [52]

relevance of the receptor variants for C1 activity, potentiation of the PP EC_{30} response was studied in presence of 10 and 30 µM of C1. Here, the Y_4R variants S1.38I, E1.42G, C2.5A, H7.39A, M7.43N, and C7.47T have a negligible effect on C1 activity, while Y1.39T and F7.35 L reduced the PAM activity of C1 by about 50% (Fig. 9A). For two variants L7.36H and L7.40K, the PAM activity is increased at a maximal concentration of 30 µM, identifying them as weak *gain-of-function* variants. Interestingly, we also identified four variants (C2.57G, Q2.58A, N7.32G, L7.36T) that markedly reduced C1 PAM activity (Fig. 9A).

In cluster 0 and 2, C1 directly interacts with the Y_4R residue Q2.58, while C1 in cluster 1 is not involved in interactions with Q2.58 (Fig. 8B – D). Mutation to Ala in cluster 0 and 2 might disturb the polar interaction and consequently weakens the Y_4R-PAM interaction (Fig. 9B). Additionally, mutation of the Cys residue at position 2.57 to Gly hampers the activity of C1 at Y_4R in activity studies (Fig. 9A). Gly residues in the 7TM domain are known as 'helix breaker' [53, 54]. Thus, this mutation might destabilize the helical structure and might interrupt nearby interactions of C1 with Y_4R (e.g. polar interaction with Q2.58 in cluster 2), which can strongly reduce the activity of the compound (Fig. 9A). Another *loss-of-function* Y_4R variant is N7.32G. Here, the Gly residue might destabilize the C1-PP-Y_4R interaction, indicating that the polar Asn residue is relevant at this position, even if it is not involved in a direct interaction with C1. The Y_4R variants L7.36H and L7.40K were predicted as *gain-of-function* variants for C1 activity. We have shown that a concentration of 10 µM of C1 potentiated

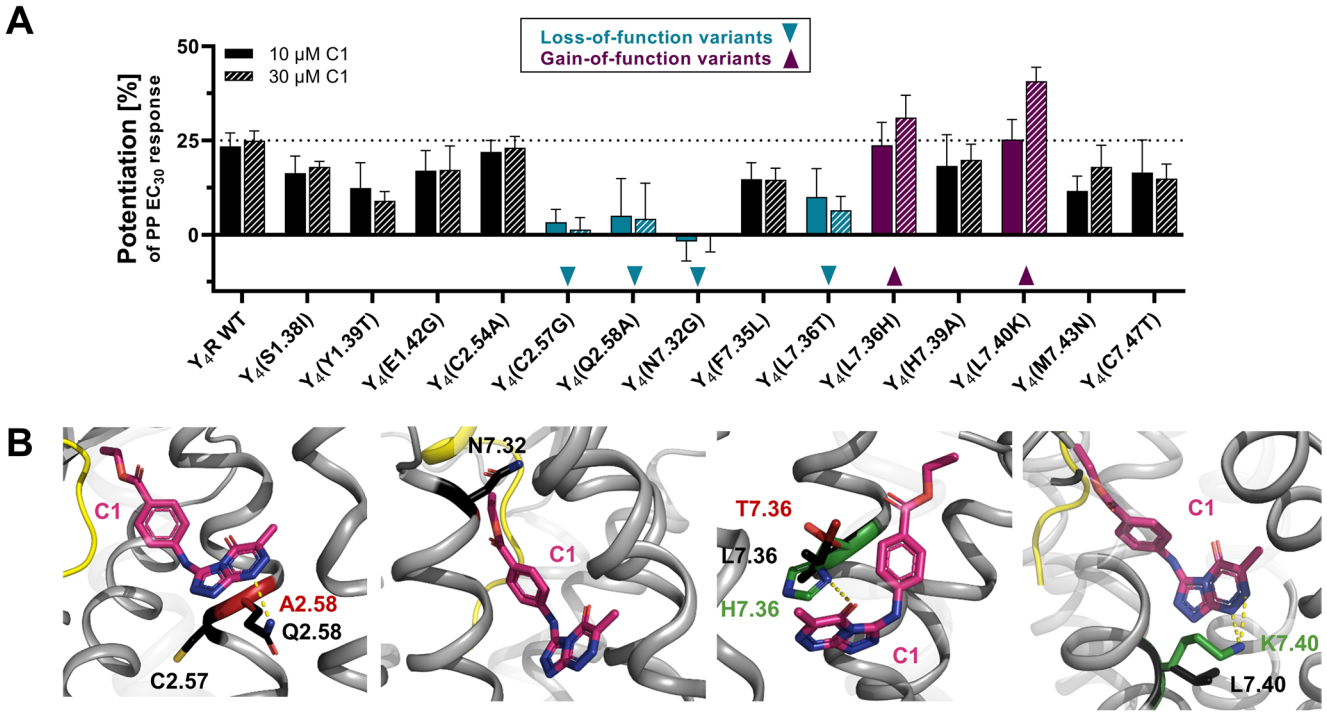


Fig. 9 PAM effect of C1 at new Y_4R variants. (**A**) Potentiation of the PP EC_{30} response at novel Y_4R variants in the presence of 10 and 30 µM of C1 investigated by Ca^{2+} flux assay in COS-7 cells transiently expressing Y_4R or variants and the chimeric G protein $\Delta 6G\alpha_{qi4\text{-}myr}$. Data are shown as mean ± SEM from $N \geq 3$ independent experiments. Variants, at which the PAM effect of C1 is lost, are highlighted in cyan and designated as *loss-of-function* variants, while variants with improved potentiation of the PP response are referred to as *gain-of-function* variants and are colored in purple. (**B**) Verification of *loss-of-function* and *gain-of-function* variants for the PAM C1 in the most likely binding cluster of C1 (cluster 2). The compound is shown in pink stick representation, Y_4R is shown as grey cartoon. Specific Y_4R residues are shown as sticks: black – native residue, green – *gain-of-function* variant, red – *loss-of-function* variant. Polar interactions are shown as dashed yellow lines

PP-mediated Y_4R response by 25% at H7.36 comparable to the WT receptor, whereas 30 µM of C1 increased the PAM activity to 30%. In contrast, a Thr mutant at position 7.36 reduced the PAM activity of C1 (Fig. 9A), highlighting the importance of this position for the compound. As shown in Fig. 9B, His at position 7.36 might form an additional polar bond with C1 in cluster 2 and shows significant van der Waals overlaps, thus tightening the binding of the compound to its Y_4R allosteric pocket. In cluster 1, the compound binds too deep within the 7TM bundle to contact position 7.36. In cluster 0, a mutation of L7.36 to His forms van der Waals interactions with C1, but is not able to make an additional polar interaction (data not shown), strengthening the binding mode of C1 as shown in cluster 2. Another relevant position is L7.40. A Lys at position 7.40 markedly enhanced the activity of the PAM compared to the native residue Leu (Fig. 9A). In cluster 2, mutation to Lys at position 7.40 of Y_4R might form an additional polar interaction with C1, thus stabilizing the active Y_4R conformation. In conclusion, we identified several *loss-* and *gain-of-function* variants that are unique to cluster 2, supporting cluster 2 as the most likely binding mode of C1 to Y_4R.

Discussion

The Y_4R, a peptide GPCR, is involved in the regulation of critical physiological processes, including energy homeostasis, food intake, colonic transit, and gut motor function [29, 55, 56]. GPCR activation can be modulated by different types of ligands acting through orthosteric or allosteric receptor sites. Notably, Y_4R agonists or PAMs have emerged as potential anti-obesity drugs [20, 57–59]. Within the last decades, many efforts have been made to identify ligands that are selective for the Y_4R subtype, and thus forward the Y_4R as a clinically relevant drug target for metabolic disorders. Obinepitide (TM-30339, 7TM Pharma) [60], a synthetic chimeric variant of the peptides PP and PYY, acts as a dual Y_2R/Y_4R agonist and has undergone phase II clinical trials for obesity treatment. However, its peptide nature poses challenges regarding its metabolic stability and oral bioavailability in vivo. To address these issues, efforts have been made to develop stabilized PP analogs through PEGylation [61, 62] or lipidation [62–64]. Additionally, several Y_4R agonists derived from the C-terminal pentapeptide of the NPY peptides have been described. The first

peptides derived by this approach, e.g. GR231118, showed poor selectivity within the Y receptor family [65]. However, recent studies report on C-terminally-derived pentapeptides with high and selective Y_4R activity [24, 66–68]. Another promising approach is the use of Y_4R positive allosteric modulators, which precisely modulate agonist-induced Y_4R signaling through an allosteric pocket. Low-molecular weight allosteric compounds offer improved stability and bioavailability compared to unmodified peptides with reduced side effects as they enhance the effects to endogenous ligands, while maintaining native spatiotemporal signaling patterns [69, 70]. We have already reported on the identification of several Y_4R allosteric modulators. The first Y_4R PAM was niclosamide, which showed a poor Y receptor selectivity and was further reported to act as allosteric antagonist at the metabotropic glutamate 1 receptor (mGluR1) [28, 71]. Advanced Y_4R-selective allosteric modulators include the agonistic PAM (ago-PAM) tBPC and the allosteric antagonist *(S)*-VU0637120 [27, 35]. VU0506013 has been reported as Y_4R pure PAM that modulates the G-protein pathway without affecting ligand binding [39]. In this study, we identified C1 (VU0610218) as a structurally novel Y_4R PAM with nanomolar binding affinity and a high allosteric cooperativity. Compared to VU0506013, which is characterized by a higher binding affinity (K_B) to Y_4R, C1 shows a markedly improved positive allosteric cooperativity with the endogenous agonist PP. Thus, both Y_4R PAMs have different characteristics with respect to their allosteric behavior. In addition to the G-protein pathway (Figs. 1 and 3), C1 was shown to increase the efficacy of arrestin-3 recruitment to Y_4R (Fig. 5). Consequently, C1 does not exhibit pathway selectivity towards the two major pathways for GPCRs [1] and acts as potentiator at the G-protein signaling and arrestin-3 recruitment pathway. In the G-protein pathway, C1 affects the potency and efficacy of the agonist PP, while in the arrestin recruitment pathway, C1 shows an efficacy-driven effect. The increased efficacy in arrestin-3 recruitment might be due to an enhanced or stabilized binding of the peptide agonist to Y_4R, as the affinity of arrestin to the Y_4R remains unaffected by C1. In radioligand binding studies, we have further shown that C1 increases the affinity of the peptide ligands PP and PYY to Y_4R membranes. We suggest that C1 helps to stabilize the agonist-bound receptor conformation via backbone and hydrophobic interactions with P^{34} of the orthosteric peptide ligand PP (Fig. 5D), and thus might increase the residence time in the ligand-bound state. The exact mechanism of C1 PAM activity in the potentiation of PP-mediated Y_4R response, however, remains speculative. GPCRs are highly dynamic structures and can adopt multiple different conformational states during the transition from the inactive to the active state. It might be that binding of the PAM pre-forms the Y_4R binding pocket for PP, thus facilitating agonist binding and G-protein association by lowering the energy barrier for the transition to the active state and stabilizing the extracellular ligand-binding domain. Binding of the PAM C1 might further modulate the allosteric interaction network within the TM bundle that links the extracellular ligand-binding pocket and the effector coupling interface, thereby altering the conformational dynamics of the Y_4R. For the M2 muscarinic receptor (M2R), a modulator was shown to have positive allosteric effects on agonist affinity by stabilizing the extracellular domain of the receptor, mainly by changing the dynamics of the aromatic network linking the allosteric and orthosteric binding sites [72]. Another option is that a population of Y_4R is already in the active state upon binding of C1. This is supported by data from GloSensor cAMP assay (Fig. 4A). Here, the compound C1 increases the basal Y_4R activity in the absence of the peptide ligand by stabilizing the Y_4R active conformation and shifting the equilibrium towards the active state. Furthermore, binding of the PAM might also allosterically stabilize the fully active Y_4R-PP-G_i protein complex and reduce the oscillation between the active and inactive receptor state by increasing the residence time in the active state. This was recently shown by Cao et al. for a metabotropic glutamate 2 receptor (mGlu2R) PAM, in which the authors investigated the structural dynamics of mGlu2R in the presence and absence of the PAM [73]. However, to clarify the exact mechanism of C1 at Y_4R, advanced experiments are needed. An interesting aspect might be to examine the dynamics of Y_4R activation in the presence and/or absence of the PAM C1 and the NAM *(S)*-VU0637120. This might help to unveil different structural states of the Y_4R and to better understand the mechanism of positive and negative allosteric modulation at Y_4R.

Additionally, we demonstrated that C1 has a reduced allosteric effect for the low-affinity ligands NPY and PYY at Y_4R. Sequence alignments of the NPY ligands (Fig. S3B) highlight the amino acid difference at position 34 of PP (P^{34}) and NPY/PYY (Q^{34}). As mentioned above, we assume that P^{34} of the orthosteric peptide ligand PP is engaged in hydrophobic interactions with C1 and thus strengthen the allosteric interaction between C1 and PP at Y_4R. The sequence variability at position 34 appears to affect the orientation and interaction of NPY and PYY with C1 within the Y_4R binding pocket, thereby reducing the allosteric cooperativity, which is indicated by the reduced allosteric modulation (2.2-fold EC_{50} shift for NPY, 2.9-fold EC_{50} shift for PYY versus 5-fold EC_{50} shift for PP).

Another important step towards understanding the mechanism of allosteric modulators involves gaining insights into their binding modes at GPCRs. The identification of allosteric binding sites often faces many challenges, primarily due to the diverse and unpredictable nature of these sites.

Initially, we focused on the identification of Y_4R domains that are relevant for the PAM activity of C1 by using Y_4R/Y_1R chimeras. Chimeric receptors are specifically used to identify amino acid residues differing between Y_4R and Y_1R, whereas identical residues are not covered by chimeras (Fig. 2A). For that reason, additional Y_4R single mutants were selected, including residues that have previously been shown to be either important for the binding of the endogenous ligand PP [30] or the Y_4R allosteric antagonist *(S)*-VU0637120 [35]. Notably, some of the Y_4R residues identified to be relevant for the PAM C1, including T2.61, D6.59, and M7.43, have also been shown to be important for the interaction with the endogenous ligand PP. D6.59 is a highly conserved residue that is critical for all Y receptor subtypes to bind their NPY ligands [30, 31, 74]. As shown in the PP-Y_4R cryo-EM structure, an ionic interaction between D6.59 and R^{35} of PP is formed [7]. As indicated by the docking model of C1 bound to Y_4R (Fig. 8), D6.59 is not involved in direct interactions with the PAM, but seems to have a structural role in the stabilization of the PAM-bound active state structure. Furthermore, residue T2.61 has been proposed to be relevant for the interaction with C1 and PP. In the Y_4R-PP-G_{i1} cryo-EM structure, T2.61 is involved in a polar interaction network with the distal amidated Y^{36} of PP. This residue is located deep inside the TM helical region at the bottom of the PP-Y_4R binding pocket. We suggest that in the presence of the PAM, the Y_4R adopts a different conformation, shifting the orientation of T2.61 more towards TM1, which might even tighten the binding of PP to Y_4R. In this study, we have shown the high Y_4R selectivity of C1. Comparison of the most relevant Y_4R positions involved in C1 activity with Y_1R, Y_2R and Y_5R revealed that most positions are unique at Y_4R (Fig. S3A). This might strengthen the Y_4R subtype-selective effect of C1 as interacting or stabilizing residues are not present at the other Y receptors.

As demonstrated, the PAM C1 interacts with an allosteric binding pocket at Y_4R besides the C-terminal binding crevice of the agonist PP, and thus in a similar allosteric site already identified for the negative allosteric modulator *(S)*-VU0637120 and the G protein-preferring PAM VU0506013 (Fig. 10). However, these small molecules reveal significant structural and functional differences. The Y_4R allosteric antagonist *(S)*-VU0637120 binds to an allosteric pocket in the Y_4R TM core that slightly overlaps with the PP binding site and thus partially destabilizes PP binding through the interaction with PP-relevant residues, e.g. Y2.64, D2.68, Q3.32, F7.35 (Fig. 10D). Comparison of the *(S)*-VU0637120-bound Y_4R model and the PP-C1-Y_4R model further revealed clear differences in the conformation of the conserved rotamer toggle switch W6.48 and the nearby transmission switch F6.44 [75]. While these residues point inside the Y_4R binding pocket in the *(S)*-VU0637120-bound conformation, the side chains of these two residues are flipped outward towards the intracellular surface in the PAM-bound state (Fig. S5), which is associated with an intracellular opening of TM6 and an enhanced interaction with the G protein. Comparison of the *(S)*-VU0637120 and C1 (cluster 2) binding pocket shows that C1 binds deeper within the TM helical bundle in proximity to the C-terminal binding groove of PP (Fig. 10) and stabilizes the interaction with the endogenous ligand through backbone interactions (N^{28}/T^{32}) and thus allosterically enhances its activity. In this study, we have shown that C1 is able to potentiate the G-protein signaling and arrestin-3 recruitment and acts pathway-independent towards the two major GPCR signaling pathways, the activation of G proteins and interactions with arrestin [1, 76, 77]. We assume that through the binding of C1, the Y_4R-PP interaction is tightened, which results in an extended intracellular G-protein- and arrestin-coupling. In contrast to C1, the PAM VU0506013 shows a clear preference for modulating the G-protein pathway and has no effect on the binding affinity of the endogenous ligand PP [39]. VU0506013 binds to an allosteric pocket at Y_4R located deeper inside the 7TM bundle that is more orientated towards TM1. Here, a clear difference in the activity of the two PAMs at the variants Y_4(1.34–1.36_Y_1) and Y_4(T2.65A) has been identified. For C1, mutation of the residues 1.34–1.36 (Phe-Ile-Val) by the corresponding residues of Y_1R (Thr-Leu-Ala) induced a *gain-of-function* activity, presumably by increasing the polar interaction interface with C1. In contrast, mutation of Y_4(T2.65A) had no effect on C1 activity. For the previously described PAM VU0506013, both mutations led to a significant loss of PAM activity, indicating differences in the binding and mode of action of the small molecules even if they bind to similar pockets at Y_4R. In contrast to C1, which mainly acts by allosterically tightening PP binding, the PAM VU0506013 might stabilize a G-protein favored receptor conformation and thus potentiates G-protein coupling. The identification of distinct Y_4R allosteric pockets highlights that this receptor region can be precisely targeted by a very diverse set of ligands with different functional outcomes. The fine-tuning of a specific Y_4R response by distinct small allosteric compounds forwards this receptor as an important pharmacological target in anti-obesity research.

Conclusion

In conclusion, we identified a Y_4R PAM, which significantly improves the allosteric cooperativity with the native peptide ligand PP and fine-tunes Y_4R G-protein signaling in response to PP. Investigation of the close analog C2 revealed the structural importance of an ethyl acetate side chain for

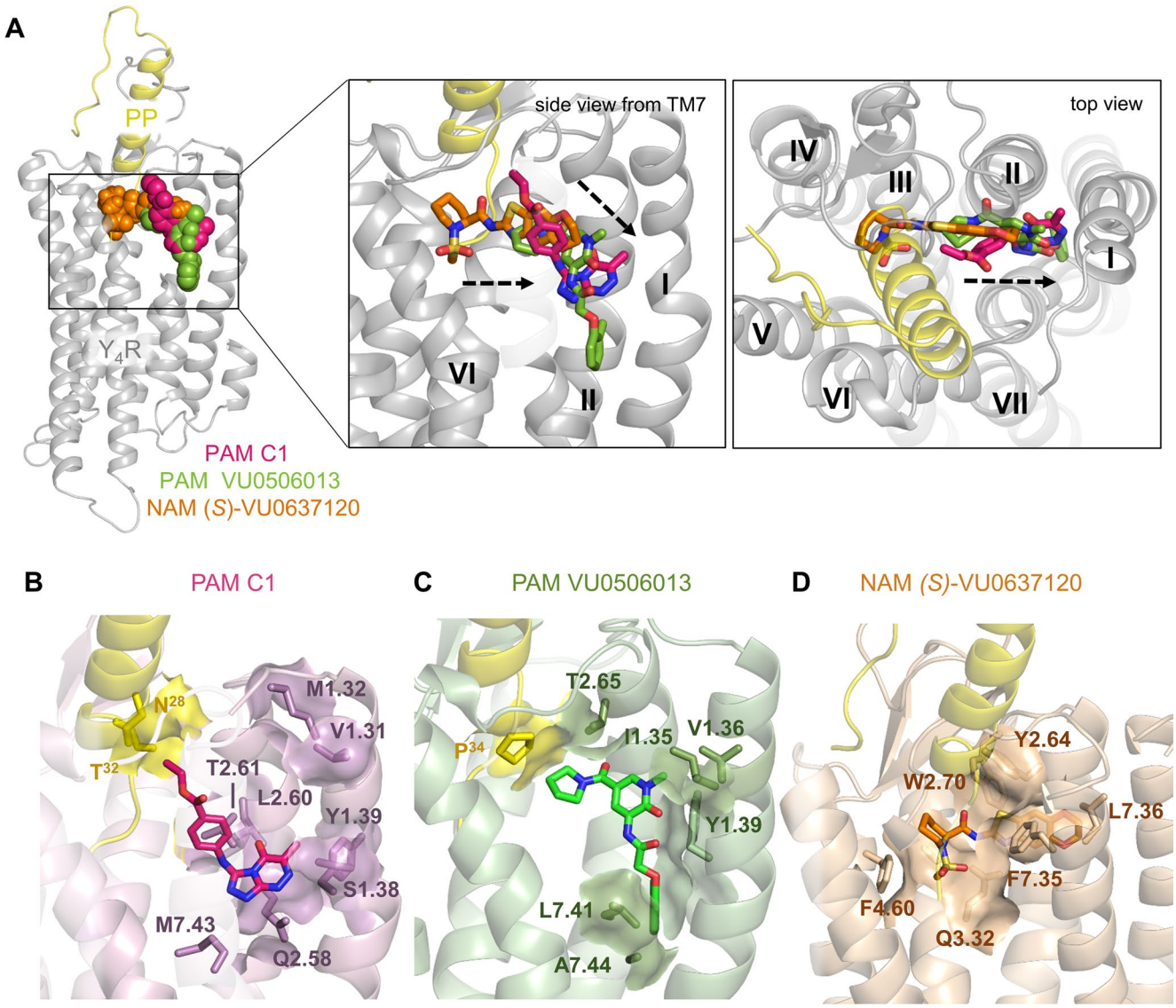


Fig. 10 Comparison of overlapping allosteric and orthosteric ligand binding pockets at Y_4R. (**A**) Overlay of the PAM C1 (cluster 2, pink sticks/spheres), PAM VU0506013 (green sticks/spheres), and NAM *(S)*-VU0637120 (orange sticks/spheres) binding sites at Y_4R. Y_4R and PP are shown in grey and yellow cartoon representation, respectively. As a template, the PP-Y_4R cryo-EM structure was used (PDB: 7X9C). (**B–D**) Detailed binding mode of the pathway-independent PAM C1 (B), the PAM VU0506013 (C) and the allosteric antagonist (*S*)-VU0637120 (D) at Y_4R. Relevant residues involved in the interaction with the small molecule are shown as sticks; the contact interface between the compounds and Y_4R residues or PP (yellow) is shown in surface representation

the high Y_4R PAM activity and affinity. The identification of a structurally important moiety makes this an interesting scaffold and might further advance structure-activity relationship (SAR) studies. Assuming binding of C1 in cluster 2, removal of the ethyl acetate moiety might destabilize PP binding by the loss of the tight backbone interactions with PP. Additionally, we identified several residues within the extracellular region of Y_4R in proximity to the endogenous ligand binding pocket that are important for C1 that might stabilize the PP-bound Y_4R active state conformation. Taken together, this compound provides an interesting scaffold for further Y_4R allosteric modulator research. For future work, it would be highly interesting to unravel the dynamics of Y_4R activation in the presence of the PAM and the orthosteric agonist.

Supplementary Information The online version contains supplementary material available at https://doi.org/10.1007/s00018-025-06019-7.

Acknowledgements The authors gratefully thank Kristin Löbner and Janet Schwesinger for their technical assistance and support. We kindly acknowledge Prof. Dr. Gunnar Schulte and Dr. Hannes Schihada for providing the G protein BRET sensor plasmids. The authors acknowledge the Vanderbilt High-throughput Screening facility where the initial HTS for identification of C1 was performed. The authors

acknowledge funding by the Deutsche Forschungsgemeinschaft (DFG, German Research Foundation) through SFB1423, project number 421152132, subproject B01 to A.G.B.-S. and A07 to J.M. J.M. is supported by a Humboldt Professorship of the Alexander von Humboldt Foundation. J.M. is supported by BMBF (Federal Ministry of Education and Research) through the Center for Scalable Data Analytics and Artificial Intelligence (ScaDS.AI). This work is partly supported by the Federal Ministry of Education and Research (BMBF) through DAAD project 57616814 (SECAI, School of Embedded Composite AI). Work in the Meiler laboratory is further supported through the NIH (R01 DA046138, S10 OD016216, S10 OD020154, S10 OD032234). This work was supported by the BMBF-funded German Network for Bioinformatics Infrastructure (de.NBI).

Author contributions Corinna Schüß planned, performed and analyzed in vitro experiments, analyzed and evaluated the experimental data, and wrote the manuscript. Oanh Vu performed and analyzed computational docking and wrote the docking method section. Tim Pelczyk performed GloSensor cAMP assays and contributed to manuscript revision. Mario Schubert analyzed and discussed experimental data, and edited the manuscript. Jan Stichel contributed to data discussion and reviewed the manuscript. Yu Du and C. David Weaver performed HTS. C. David Weaver supervised and planned HTS, analyzed HTS data, and contributed to data discussion. Jens Meiler planned and supervised docking studies, contributed to data discussion, planning of experiments and data analysis, and reviewed the manuscript. Annette G. Beck-Sickinger planned and analyzed experiments, discussed data, supervised the project, and edited the manuscript. All authors read and approved the final version of the manuscript.

Funding Open Access funding enabled and organized by Projekt DEAL. This work was supported by the Deutsche Forschungsgemeinschaft (DFG, German Research Foundation) through SFB1423, project number 421152132, subproject B01 to A.G.B.-S. and A07 to J.M. J.M. is supported by a Humboldt Professorship of the Alexander von Humboldt Foundation. J.M. is supported by BMBF (Federal Ministry of Education and Research) through the Center for Scalable Data Analytics and Artificial Intelligence (ScaDS.AI). This work is partly supported by the Federal Ministry of Education and Research (BMBF) through DAAD project 57616814 (SECAI, School of Embedded Composite AI). Work in the Meiler laboratory is further supported through the NIH (R01 DA046138, S10 OD016216, S10 OD020154, S10 OD032234). This work was supported by the BMBF-funded German Network for Bioinformatics Infrastructure (de.NBI).

Data availability Data and materials are available upon request.

Declarations

Ethics approval Not applicable.

Consent to participate Not applicable.

Consent to publish Not applicable.

Competing interests The authors declare the following competing financial interest: C.D.W. is an owner of WaveFront Biosciences, the maker of the Panoptic Plate reader used for the HTS Ca^{2+} flux experiments.

Open Access This article is licensed under a Creative Commons Attribution 4.0 International License, which permits use, sharing, adaptation, distribution and reproduction in any medium or format, as long as you give appropriate credit to the original author(s) and the source, provide a link to the Creative Commons licence, and indicate if changes were made. The images or other third party material in this article are included in the article's Creative Commons licence, unless indicated otherwise in a credit line to the material. If material is not included in the article's Creative Commons licence and your intended use is not permitted by statutory regulation or exceeds the permitted use, you will need to obtain permission directly from the copyright holder. To view a copy of this licence, visit http://creativecommons.org/licenses/by/4.0/.

References

1. Hilger D, Masureel M, Kobilka BK (2018) Structure and dynamics of GPCR signaling complexes. Nat Struct Mol Biol 25:4–12. https://doi.org/10.1038/s41594-017-0011-7
2. Hauser AS, Attwood MM, Rask-Andersen M et al (2017) Trends in GPCR drug discovery: new agents, targets and indications. Nat Rev Drug Discov 16:829–842. https://doi.org/10.1038/nrd.2017.178
3. Isberg V, Mordalski S, Munk C et al (2016) GPCRdb: an information system for G protein-coupled receptors. Nucleic Acids Res 44:356–364. https://doi.org/10.1093/nar/gkv1178
4. Davenport AP, Scully CCG, de Graaf C et al (2020) Advances in therapeutic peptides targeting G protein-coupled receptors. Nat Rev Drug Discov 19:389–413. https://doi.org/10.1038/s41573-020-0062-z
5. Henninot A, Collins JC, Nuss JM (2018) The current state of peptide drug discovery: back to the future? J Med Chem 61:1382–1414. https://doi.org/10.1021/acs.jmedchem.7b00318
6. Christopoulos A (2002) Allosteric binding sites on cell-surface receptors: novel targets for drug discovery. Nat Rev Drug Discov 1:198–210. https://doi.org/10.1038/nrd746
7. Tang T, Tan Q, Han S et al (2022) Receptor-specific recognition of NPY peptides revealed by structures of NPY receptors. Sci Adv 8:eabm1232. https://doi.org/10.1126/sciadv.abm1232
8. Lu S, Zhang J (2019) Small molecule allosteric modulators of G-protein-coupled receptors: drug-target interactions. J Med Chem 62:24–45. https://doi.org/10.1021/acs.jmedchem.7b01844
9. Christopoulos A, Kenakin T (2002) G protein-coupled receptor allosterism and complexing. Pharmacol Rev 54:323–374
10. May LT, Leach K, Sexton PM et al (2007) Allosteric modulation of G protein-coupled receptors. Annu Rev Pharmacol Toxicol 47:1–51. https://doi.org/10.1146/annurev.pharmtox.47.120505.105159
11. Messa P, Alfieri C, Brezzi B (2008) Cinacalcet: pharmacological and clinical aspects. Expert Opin Drug Metab Toxicol 4:1551–1560. https://doi.org/10.1517/17425250802587017
12. Lindberg JS, Culleton B, Wong G et al (2005) Cinacalcet HCl, an oral calcimimetic agent for the treatment of secondary hyperparathyroidism in hemodialysis and peritoneal dialysis: a randomized, double-blind, multicenter study. J Am Soc Nephrol 16:800–807. https://doi.org/10.1681/ASN.2004060512
13. Dorr P, Westby M, Dobbs S et al (2005) Maraviroc (UK-427,857), a potent, orally bioavailable, and selective small-molecule inhibitor of chemokine receptor CCR5 with broad-spectrum anti-human immunodeficiency virus type 1 activity. Antimicrob Agents Chemother 49:4721–4732. https://doi.org/10.1128/AAC.49.11.4721-4732.2005
14. Liu H, Kim HR, Deepak RNVK et al (2018) Orthosteric and allosteric action of the C5a receptor antagonists. Nat Struct Mol Biol 25:472–481. https://doi.org/10.1038/s41594-018-0067-z
15. Shen S, Zhao C, Wu C et al (2023) Allosteric modulation of G protein-coupled receptor signaling. Front Endocrinol 14:1137604. https://doi.org/10.3389/fendo.2023.1137604

16. Feng Z, Hu G, Ma S et al (2015) Computational advances for the development of allosteric modulators and bitopic ligands in G protein-coupled receptors. AAPS J 17:1080–1095. https://doi.org/10.1208/s12248-015-9776-y
17. Lu S, Huang W, Zhang J (2014) Recent computational advances in the identification of allosteric sites in proteins. Drug Discov Today 19:1595–1600. https://doi.org/10.1016/j.drudis.2014.07.012
18. Lundell I, Blomqvist AG, Berglund MM et al (1995) Cloning of a human receptor of the NPY receptor family with high affinity for pancreatic polypeptide and peptide YY. J Biol Chem 270:29123–29128. https://doi.org/10.1074/jbc.270.49.29123
19. Asakawa A, Inui A, Yuzuriha H et al (2003) Characterization of the effects of pancreatic polypeptide in the regulation of energy balance. Gastroenterology 124:1325–1336. https://doi.org/10.1016/s0016-5085(03)00216-6
20. Schüß C, Behr V, Beck-Sickinger AG (2024) Illuminating the neuropeptide Y4 receptor and its ligand pancreatic polypeptide from a structural, functional, and therapeutic perspective. Neuropeptides 105:102416. https://doi.org/10.1016/j.npep.2024.102416
21. Schwartz TW (1983) Pancreatic polypeptide: a hormone under vagal control. Gastroenterology 85:1411–1425
22. Li J-B, Asakawa A, Terashi M et al (2010) Regulatory effects of Y4 receptor agonist (BVD-74D) on food intake. Peptides 31:1706–1710. https://doi.org/10.1016/j.peptides.2010.06.011
23. Ueno N, Inui A, Iwamoto M et al (1999) Decreased food intake and body weight in pancreatic polypeptide-overexpressing mice. Gastroenterology 117:1427–1432. https://doi.org/10.1016/S0016-5085(99)70293-3
24. Balasubramaniam A, Mullins DE, Lin S et al (2006) Neuropeptide Y (NPY) Y4 receptor selective agonists based on NPY(32–36): development of an anorectic Y4 receptor selective agonist with picomolar affinity. J Med Chem 49:2661–2665. https://doi.org/10.1021/jm050907d
25. Jesudason DR, Monteiro MP, McGowan BMC et al (2007) Low-dose pancreatic polypeptide inhibits food intake in man. Br J Nutr 97:426–429. https://doi.org/10.1017/S0007114507336799
26. Batterham RL, Le Roux CW, Cohen MA et al (2003) Pancreatic polypeptide reduces appetite and food intake in humans. J Clin Endocrinol Metab 88:3989–3992. https://doi.org/10.1210/jc.2003-030630
27. Schubert M, Stichel J, Du Y et al (2017) Identification and characterization of the first selective Y4 receptor positive allosteric modulator. J Med Chem 60:7605–7612. https://doi.org/10.1021/acs.jmedchem.7b00976
28. Sliwoski G, Schubert M, Stichel J et al (2016) Discovery of small-molecule modulators of the human Y4 receptor. PLoS One 11:e0157146. https://doi.org/10.1371/journal.pone.0157146
29. Pedragosa-Badia X, Stichel J, Beck-Sickinger AG (2013) Neuropeptide Y receptors: how to get subtype selectivity. Front Endocrinol 4:5. https://doi.org/10.3389/fendo.2013.00005
30. Pedragosa-Badia X, Sliwoski GR, Dong Nguyen E et al (2014) Pancreatic polypeptide is recognized by two hydrophobic domains of the human Y4 receptor binding pocket. J Biol Chem 289:5846–5859. https://doi.org/10.1074/jbc.M113.502021
31. Merten N, Lindner D, Rabe N et al (2007) Receptor subtype-specific docking of Asp6.59 with C-terminal arginine residues in Y receptor ligands. J Biol Chem 282:7543–7551. https://doi.org/10.1074/jbc.M608902200
32. Kostenis E (2001) Is Gα16 the optimal tool for fishing ligands of orphan G-protein-coupled receptors? Trends Pharmacol Sci 22:560–564. https://doi.org/10.1016/S0165-6147(00)01810-1
33. Mäde V, Babilon S, Jolly N et al (2014) Peptide modifications differentially alter G protein-coupled receptor internalization and signaling bias. Angew Chem 53:10067–10071. https://doi.org/10.1002/anie.201403750
34. Walther C, Nagel S, Gimenez LE et al (2010) Ligand-induced internalization and recycling of the human neuropeptide Y2 receptor is regulated by its carboxyl-terminal tail. J Biol Chem 285:41578–41590. https://doi.org/10.1074/jbc.M110.162156
35. Schüß C, Vu O, Schubert M et al (2021) Highly selective Y4 receptor antagonist binds in an allosteric binding pocket. J Med Chem 64:2801–2814. https://doi.org/10.1021/acs.jmedchem.0c02000
36. Aurelio L, Valant C, Flynn BL et al (2009) Allosteric modulators of the adenosine A1 receptor: synthesis and pharmacological evaluation of 4-substituted 2-amino-3-benzoylthiophenes. J Med Chem 52:4543–4547. https://doi.org/10.1021/jm9002582
37. Schihada H, Shekhani R, Schulte G (2021) Quantitative assessment of constitutive G protein-coupled receptor activity with BRET-based G protein biosensors. Sci Signal 14:eabf1653. https://doi.org/10.1126/scisignal.abf1653
38. Bradford MM (1976) A rapid and sensitive method for the quantitation of microgram quantities of protein utilizing the principle of protein-dye binding. Anal Biochem 72:248–254. https://doi.org/10.1006/abio.1976.9999
39. Schüß C, Vu O, Mishra NM et al (2023) Structure-activity relationship study of the high-affinity neuropeptide Y4 receptor positive allosteric modulator VU0506013. J Med Chem 66:8745–8766. https://doi.org/10.1021/acs.jmedchem.3c00383
40. Leman JK, Weitzner BD, Lewis SM et al (2020) Macromolecular modeling and design in rosetta: recent methods and frameworks. Nat Methods 17:665–680. https://doi.org/10.1038/s41592-020-0848-2
41. Alam N, Goldstein O, Xia B et al (2017) High-resolution global peptide-protein docking using fragments-based PIPER-FlexPepDock. PLoS Comput Biol 13:e1005905. https://doi.org/10.1371/journal.pcbi.1005905
42. Brown BP, Vu O, Geanes AR et al (2022) Introduction to the biochemical library (BCL): an application-based open-source toolkit for integrated cheminformatics and machine learning in computer-aided drug discovery. Front Pharmacol 13:833099. https://doi.org/10.3389/fphar.2022.833099
43. Kothiwale S, Mendenhall JL, Meiler J (2015) BCL:Conf: small molecule conformational sampling using a knowledge based rotamer library. J Cheminform 7:47. https://doi.org/10.1186/s13321-015-0095-1
44. Mendenhall J, Brown BP, Kothiwale S et al (2021) BCL:Conf: improved open-source knowledge-based conformation sampling using the crystallography open database. J Chem Inf Model 61:189–201. https://doi.org/10.1021/acs.jcim.0c01140
45. Meiler J, Baker D (2006) ROSETTALIGAND: protein-small molecule docking with full side-chain flexibility. Proteins 65:538–548. https://doi.org/10.1002/prot.21086
46. Lemmon G, Meiler J (2012) Rosetta ligand docking with flexible XML protocols. Methods Mol Biol 819:143–155. https://doi.org/10.1007/978-1-61779-465-0_10
47. Moretti R, Bender BJ, Allison B et al (2016) Rosetta and the design of ligand binding sites. Methods Mol Biol 1414:47–62. https://doi.org/10.1007/978-1-4939-3569-7_4
48. Kenakin T (2017) A scale of agonism and allosteric modulation for assessment of selectivity, bias, and receptor mutation. Mol Pharmacol 92:414–424. https://doi.org/10.1124/mol.117.108787
49. Fan F, Binkowski BF, Butler BL et al (2008) Novel genetically encoded biosensors using firefly luciferase. ACS Chem Biol 3:346–351. https://doi.org/10.1021/cb8000414
50. Chen G, Way J, Armour S et al (2000) Use of constitutive G protein-coupled receptor activity for drug discovery. Mol Pharmacol 57:125–134. https://doi.org/10.1016/S0026-895X(24)26450-6

51. Wanka L, Babilon S, Burkert K et al (2017) C-terminal motif of human neuropeptide Y4 receptor determines internalization and arrestin recruitment. Cell Signal 29:233–239. https://doi.org/10.1016/j.cellsig.2016.11.003
52. Ballesteros JA, Weinstein H (1995) Integrated methods for the construction of three-dimensional models and computational probing of structure-function relations in G protein-coupled receptors. Methods Neurosciences 25:366–428. https://doi.org/10.1016/S1043-9471(05)80049-7
53. Dong H, Sharma M, Zhou H-X et al (2012) Glycines: role in α-helical membrane protein structures and a potential indicator of native conformation. Biochemistry 51:4779–4789. https://doi.org/10.1021/bi300090x
54. Javadpour M M., Eilers M, Groesbeek M et al (1999) Helix packing in polytopic membrane proteins: role of glycine in transmembrane helix association. Biophys J 77:1609–1618. https://doi.org/10.1016/S0006-3495(99)77009-8
55. Asakawa A, Inui A, Ueno N et al (1999) Mouse pancreatic polypeptide modulates food intake, while not influencing anxiety in mice☆. Peptides 20:1445–1448. https://doi.org/10.1016/S0196-9781(99)00155-2
56. Moriya R, Fujikawa T, Ito J et al (2010) Pancreatic polypeptide enhances colonic muscle contraction and fecal output through neuropeptide Y Y4 receptor in mice. Eur J Pharmacol 627:258–264. https://doi.org/10.1016/j.ejphar.2009.09.057
57. Kamiji MM, Inui A (2007) NPY Y2 and Y4 receptors selective ligands: promising anti-obesity drugs? Curr Top Med Chem 7:1734–1742. https://doi.org/10.2174/156802607782340957
58. Brothers SP, Wahlestedt C (2010) Therapeutic potential of neuropeptide Y (NPY) receptor ligands. EMBO Mol Med 2:429–439. https://doi.org/10.1002/emmm.201000100
59. Sato N, Ogino Y, Mashiko S et al (2009) Modulation of neuropeptide Y receptors for the treatment of obesity. Expert Opin Ther Pat 19:1401–1415. https://doi.org/10.1517/13543770903251722
60. Schwartz T (2005) Y4 selective receptor agonists for therapeutic interventions. Patent WO2005089786 (A2), 29 Sept 2005
61. Lumb K, Decarr L (2006) Neuropeptide Y4 receptor agonists. Patent WO2006/091506 (A2), 31 Aug 2006
62. Bellmann-Sickert K, Elling CE, Madsen AN et al (2011) Long-acting lipidated analogue of human pancreatic polypeptide is slowly released into circulation. J Med Chem 54:2658–2667. https://doi.org/10.1021/jm101357e
63. Mäde V, Bellmann-Sickert K, Kaiser A et al (2014) Position and length of fatty acids strongly affect receptor selectivity pattern of human pancreatic polypeptide analogues. ChemMedChem 9:2463–2474. https://doi.org/10.1002/cmdc.201402235
64. Verma D, Hörmer B, Bellmann-Sickert K et al (2016) Pancreatic polypeptide and its central Y4 receptors are essential for cued fear extinction and permanent suppression of fear. Br J Pharmacol 173:1925–1938. https://doi.org/10.1111/bph.13456
65. Parker EM, Babij CK, Balasubramaniam A et al (1998) GR231118 (1229U91) and other analogues of the C-terminus of neuropeptide Y are potent neuropeptide Y Y1 receptor antagonists and neuropeptide Y Y4 receptor agonists. Eur J Pharmacol 349:97–105. https://doi.org/10.1016/s0014-2999(98)00171-x
66. Kuhn KK, Ertl T, Dukorn S et al (2016) High affinity agonists of the neuropeptide Y (NPY) Y4 receptor derived from the C-terminal pentapeptide of human pancreatic polypeptide (hPP): synthesis, stereochemical discrimination, and radiolabeling. J Med Chem 59:6045–6058. https://doi.org/10.1021/acs.jmedchem.6b00309
67. Konieczny A, Braun D, Wifling D et al (2020) Oligopeptides as neuropeptide Y Y4 receptor ligands: identification of a high-affinity tetrapeptide agonist and a hexapeptide antagonist. J Med Chem 63:8198–8215. https://doi.org/10.1021/acs.jmedchem.0c00426
68. Konieczny A, Conrad M, Ertl FJ et al (2021) N-terminus to arginine side-chain cyclization of linear peptidic neuropeptide Y Y4 receptor ligands results in picomolar binding constants. J Med Chem 64:16746–16769. https://doi.org/10.1021/acs.jmedchem.1c01574
69. Renukuntla J, Vadlapudi AD, Patel A et al (2013) Approaches for enhancing oral bioavailability of peptides and proteins. Int J Pharm 447:75–93. https://doi.org/10.1016/j.ijpharm.2013.02.030
70. Brown TD, Whitehead KA, Mitragotri S (2020) Materials for oral delivery of proteins and peptides. Nat Rev Mater 5:127–148. https://doi.org/10.1038/s41578-019-0156-6
71. Ai N, Wood RD, Yang E et al (2016) Niclosamide is a negative allosteric modulator of group I metabotropic glutamate receptors: implications for neuropathic pain. Pharm Res 33:3044–3056. https://doi.org/10.1007/s11095-016-2027-9
72. Xu J, Wang Q, Hübner H et al (2023) Structural and dynamic insights into supra-physiological activation and allosteric modulation of a muscarinic acetylcholine receptor. Nat Commun 14:376. https://doi.org/10.1038/s41467-022-35726-z
73. Cao A-M, Quast RB, Fatemi F et al (2021) Allosteric modulators enhance agonist efficacy by increasing the residence time of a GPCR in the active state. Nat Commun 12:5426. https://doi.org/10.1038/s41467-021-25620-5
74. Rudolf S, Kaempf K, Vu O et al (2021) Binding of natural peptide ligands to the neuropeptide Y5 receptor. Angew Chem Int Ed Engl 61:e202108738. https://doi.org/10.1002/anie.202108738
75. Filipek S (2019) Molecular switches in GPCRs. Curr Opin Struct Biol 55:114–120. https://doi.org/10.1016/j.sbi.2019.03.017
76. Shenoy SK, Lefkowitz RJ (2011) β-arrestin-mediated receptor trafficking and signal transduction. Trends Pharmacol Sci 32:521–533. https://doi.org/10.1016/j.tips.2011.05.002
77. Zhang M, Chen T, Lu X et al (2024) G protein-coupled receptors (GPCRs): advances in structures, mechanisms, and drug discovery. Signal Transduct Target Ther 9:88. https://doi.org/10.1038/s41392-024-01803-6

Publisher's note Springer Nature remains neutral with regard to jurisdictional claims in published maps and institutional affiliations.